DEPARTMENT OF ELECTRICAL ENGINEERING
INDIAN INSTITUTE OF TECHNOLOGY MADRAS
CHENNAI – 600036

Role of Constellation Shaping in improving Spectral Efficiency in Satellite Communications

A Thesis

Submitted by

PRANJALI VATSALAYA

For the award of the degree

Of

MASTER OF TECHNOLOGY

June 2022

DEPARTMENT OF ELECTRICAL ENGINEERING
INDIAN INSTITUTE OF TECHNOLOGY MADRAS
CHENNAI – 600036

Role of Constellation Shaping in improving Spectral Efficiency in Satellite Communications

A Thesis

Submitted by

PRANJALI VATSALAYA

For the award of the degree

Of

MASTER OF TECHNOLOGY

June 2022

THESIS CERTIFICATE

This is to undertake that the Thesis titled **ROLE OF CONSTELLATION SHAPING IN IMPROVING SPECTRAL EFFICIENCY IN SATELLITE COMMUNICATIONS**, submitted by me, **Pranjali Vatsalaya**, to the Indian Institute of Technology Madras, for the award of **Master of Technology**, is a bonafide record of the research work done by me under the supervision of **Dr. K Giridhar**. The contents of this Thesis, in full or in parts, have not been submitted to any other Institute or University for the award of any degree or diploma.

Chennai 600036 **Pranjali Vatsalaya**

Date: June 2022 **EE17B144**

Dr. K Girdhar
Research Supervisor
Professor
Department of Electrical Engineering
IIT Madras

ACKNOWLEDGEMENTS

I want to take this opportunity to express my sincere gratitude to Dr. K Giridhar for his continuous support, invaluable insights, and constant encouragement throughout this project. The project allowed me to interact with the industry, understand their requirements, and meet them. It broadened my scope of understanding of even the basic principles and pushed me to pursue research in this direction. I would also like to express my profound gratitude to all professors of the Electrical Engineering Department who have imparted knowledge and have motivated me to learn the intricacies of the subjects.

Special thanks to Mr. Krishna Madan for his steady support and guidance. I thank my friends and labmates Dibyajyoti, Shruti, Shubham, Ravi, Leeshma, Amal, and Sai Teja for their help and encouragement. I also extend my gratitude to Nikita Tanwar, Nitin Chauhan, and Ramakrishna, who worked on the RCS project before me, for giving us a foundation to build on.

I want to take this opportunity to thank my parents and sister for their support and encouragement. Without them, becoming a part of such a prestigious institution would not have been possible. This work is dedicated to all of them.

ABSTRACT

KEYWORDS Bit-level LLRs; Turbo Codes; Constellation shaping; Relay systems; phase error correction

The flow of the thesis is two parted. The first part describes the role of using Constellation shaping in interference scenarios in Relay systems. We observe an improvement in Spectral efficiency when constellation shaping is used along with LLRs and Turbo codes. We use joint LLR and reference constellation techniques to generate LLRs. The performance enhancement is proven by modelling both interference and non-interference scenarios in a Two-phase Three-way relay system for the same system-level throughput and power per user. Their BER, BLER, and PAPR are plotted and analyzed. An extension of this to Two-phase N-way relay system is also proposed by utilizing constellation shaping benefits.

The second part of the thesis covers my role in a Satellite communication project in collaboration with DRDO. The Reliable and Covert Satellite (RCS) Communication System's primary goal is to provide reliable communications along with a low probability of detection and interception. The system can support up to 32 users spread over vast geographical areas and connected to a ground station (Hub) via a geostationary satellite. This thesis presents an overview of the forward link and reverse link design with a variation of using Turbo codes over the previously used Matrix Parity Check codes for better performance. Turbo codes have performed significantly better in all possible channel conditions, including introducing CFO error. While a companion thesis (by Shubham) describes the forward link, this thesis concerns the reverse link design and performance. A part of this project is also extended to understand the different techniques (like assumed Gaussian noise method, partial statistics method, joint-PDF method, and MaxLogMAP) to calculate bit-level LLRs in a DQPSK modulation scenario. A comparison study has been made, highlighting the best technique with lesser computations.

CONTENTS

Page

ACKNOWLEDGEMENTS **i**

ABSTRACT **iii**

LIST OF TABLES **vii**

LIST OF FIGURES **ix**

ABBREVIATIONS **xi**

CHAPTER 1 INTRODUCTION **1**

CHAPTER 2 RELAY SYSTEMS IN SATELLITE COMMUNICATIONS **3**

2.1 Introduction . . . 3
2.2 Role of Constellation Shaping in interference channel . . . 4
2.3 NO INTERFERENCE Model . . . 7
2.4 Interference Model . . . 7
2.4.1 Joint-LLR approach for interference channel . . . 7
2.4.2 Decoding at Hub's end . . . 8
2.4.3 Decoding at UE's end . . . 12
2.5 Simultaneous joint-LLR with no ideal self cancellation . . . 15
2.6 Final Comparison . . . 17
2.7 Extension to N-way relay system . . . 19

CHAPTER 3 RELIABLE AND COVERT SATELLITE COMMUNICATION SYSTEM **21**

3.1 Introduction . . . 21
3.2 Forward Link Overview . . . 23
3.2.1 FL: Transmitter block . . . 23
3.2.2 FL: Receiver block . . . 24
3.3 Reverse Link Overview . . . 24
3.3.1 RL: Transmitter block . . . 24
3.3.2 RL: Receiver block . . . 25
3.3.3 RL Frame Structure while using Turbo codes . . . 27

CHAPTER 4 SIMULATION RESULTS FOR RCS **31**

4.1 System Model . . . 31
4.2 Scenario 1 . . . 32
4.2.1 Results . . . 32
4.3 Scenario 2 . . . 34
4.3.1 Results . . . 34

4.4 Scenario 3 38
4.4.1 Results 38
4.5 Scenario 4 42
4.5.1 Results 42

CHAPTER 5 DQPSK AND LLRS 47

5.1 Introduction 47
5.1.1 Gaussian noise LLR 47
5.1.2 Partial Statistics LLR 48
5.1.3 Joint pdf LLR 49
5.1.4 Max-log MAP with joint pdf LLR 49
5.2 Simulation Results 52
5.2.1 Observations 52

CHAPTER 6 CONCLUSION 55

APPENDIX A TURBO CODES 57

A.1 Introduction 57
A.2 Turbo Encoder 57
A.3 Log-likelihood Ratios 59
A.4 Turbo Decoder 59

REFERENCES 61

LIST OF TABLES

Table	Caption	Page
2.1	Relay system specifications	9
4.1	RCS simulation system specifications	31

LIST OF FIGURES

Figure	Caption	Page
2.1	Four-phase Three-way Relay system	3
2.2	Two-phase Three-way Relay system	4
2.3	Average uncoded BER for different gain ratios	5
2.4	0.5*QPSK + QPSK super-constellation	5
2.5	0.5*QPSK + 2*$\sqrt{1.25}$*16QAM super-constellation	6
2.6	0.5*QPSK + QPSK + 2*QPSK super-constellation	6
2.7	No interference scenario	7
2.8	Signal received by hub after self-cancellation	8
2.9	Uncoded average BER for model 1 and 2 at Hub's end	9
2.10	PAPR comparison when user sends QPSK vs 16QAM	10
2.11	Coded and Uncoded BER for Model 2 with random phase error	11
2.12	Average BER of UE and hub for QPSK with gain 0.5 and gain 1	13
2.13	Average BER of UE and Hub as decoded by the other UE	14
2.14	64QAM Super-constellation formed from 3 QPSK signals	15
2.15	Simultaneous decoding of all three signals	16
2.16	Interference model comparison with and without self-cancellation	17
2.17	Improvement in Spectral Efficiency	18
2.18	Two-phase N-way Relay	19
3.1	RCS FDD layout	22
3.2	RCS FDD layout	23
3.3	FL Transmitter block	24
3.4	FL Receiver block	25
3.5	RL Transmitter block	26
3.6	RL Receiver block	27
3.7	RL Frame structure for 1/2 code rate	28
3.8	RL Frame structure for 2/3 code rate	29
4.1	Average BER for Scenario 1	32
4.2	Average BLER for Scenario 1	33
4.3	Average BER for Scenario 2 for rate 1/2	34
4.4	Average BLER for Scenario 2 for rate 1/2	35
4.5	Average BER for Scenario 2 for rate 2/3	36
4.6	Average BLER for Scenario 2 for rate 2/3	37
4.7	Average BER for Scenario 3 for rate 1/2	38
4.8	Average BLER for Scenario 3 for rate 1/2	39
4.9	Average BER for Scenario 3 for rate 2/3	40
4.10	Average BLER for Scenario 3 for rate 2/3	41
4.11	Average BER for Scenario 4 for rate 1/2	42
4.12	Average BLER for Scenario 4 for rate 1/2	43
4.13	Average BER for Scenario 4 for rate 2/3	44

4.14 Average BLER for Scenario 4 for rate 2/3 45

5.1 All possible consecutive symbols for a particular bit and position value . 51
5.2 Uncoded BER for different LLR methods 53
5.3 Coded BER for different LLR methods 54

A.1 Turbo encoder for rate $\frac{1}{3}$ 58
A.2 Turbo decoder 60

ABBREVIATIONS

BER	Bit Error Rate.
BLER	Block Error Rate.
CCE	Continous Channel Estimation.
CFO	Carrier Frequency Offset.
CFR	Channel Frequency Response.
DQPSK	differential-QPSK.
DS CDMA	Direct Sequence Code Division Multiple Access.
FDD	Frequency Division Duplex.
FEC	Forward Error Correction Codes.
FFT	Fast Fourier Transform.
FL	Forward Link.
IBI	Inter Block Interference.
LLR	Log-Likelihood Ratio.
MPCC	Matrix Parity Check Code.
OFDM	Orthogonal Frequency Division Multiplexing.
PAPR	Peak to Average Power Ratio.
PRACH	Physical Random Access Channel.
QAM	Quadrature Amplitude Modulation.
QPSK	Quadrature Phase Shift Keying.
RCS	Reliable and Covert Satellite.
RL	Reverse Link.

RSC Recursive Systematic Convolutional codes.

SI OFDMA Spread and Interleaved OFDMA.

SINR Signal to Interference and Noise Ratio.

SNR Signal to Noise Ratio.

TCC Turbo Control Codes.

UE User Equipment.

ZFE Zero-forcing Equalizer.

CHAPTER 1

INTRODUCTION

Communication systems like cellular and satellite represent information as a sequence of binary digits. The binary message is modulated to an analog signal and transmitted over a communication channel affected by noise that corrupts the transmitted signal. The channel coding, such as turbo codes, protects the information from noise and reduces the number of error bits. The performances of the turbo codes are due to parallel concatenation of component codes, the interleaver schemes, and the iterative decoding using the Soft Input Soft Output (SISO) algorithms. This, when coupled with soft-decoded values as inputs, further helps improve performance.

This thesis aims to highlight the advantages of using Turbo codes with log-likelihood ratios as inputs. This is shown under different projects. The first system model covered in Chapter 2 is a Two-phase Three-way Relay System in a Satellite environment with a hub and two users connected via a satellite. The merit of an additional constellation shaping along with LLRs and Turbo codes to enhance Spectral Efficiency is discussed. A detailed analysis of how the received signal is decoded at both the user and hub's end is done, and different solutions based on the application of the relay system are proposed. 16QAM and 64QAM super-constellations are exploited. System-level throughput and power consumption per user are kept constant across the solutions for easier comparison. Both self-cancellation and no ideal self cancellation cases are modeled and it is shown that constellation shaping, helps us achieve same performance in both cases.

In Chapter 3, we discuss a defense-satellite communication system model, which was done in collaboration with Defence Electronics Application Laboratory (DEAL), DRDO. The Reliable and Covert Satellite (RCS) Communication system is a satellite

communication air interface that can provide robust communication with minimum probability of detection and interception with moderate complexity concerning hardware and algorithms. This work combines different techniques like single-carrier block modulated DS CDMA and Interleaved OFDM for orthogonal multiple access. The chapter gives a brief overview of the Forward link, followed by an in-depth analysis of the Reverse link and all the system-level changes to accommodate TCC. In chapter 4, we highlight the advantages we get by using LLRs and Turbo codes instead of the existing MPCC codes in all possible channel conditions (timing offset, residual frequency error, difference in power of each user, and AWGN noise).

Chapter 5 reviews the MAP, Max-Log-MAP, a novel partial statistics method, and joint-pdf method as bit-level LLR computation algorithms. We extend these techniques to a differential-QPSK modulation system and compare their performance by comparing the coded and uncoded BER.

CHAPTER 2

RELAY SYSTEMS IN SATELLITE COMMUNICATIONS

2.1 INTRODUCTION

Consider a 2-phase 3-way Relay system with 2 users, 1 hub and 1 satellite. Conventionally, in satellite communication, first the signal from one user goes to the hub via the satellite and then the hub processes the signal and sends it to the destined user via satellite. This involves 4 hops.

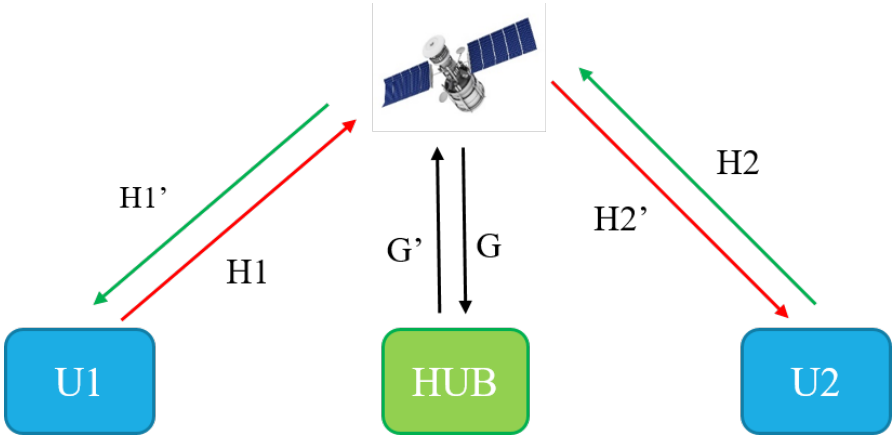

Figure 2.1: Four-phase Three-way Relay system

We aim to propose a solution in which the 2 users and hub simultaneously send their signals to the satellite and the satellite adds all the signals and send them back to each user and the hub.

The signal received by user 1, is

$$r_1 = H_1'.(s_1.H_1 + s_2.H_2 + s_G.H_G) + w$$

which simplifies to,

$$r_1 = (H_1'.H_1.s_1) + (H_1'.H_2.s_2) + (H_1'.H_G.s_G) + w$$

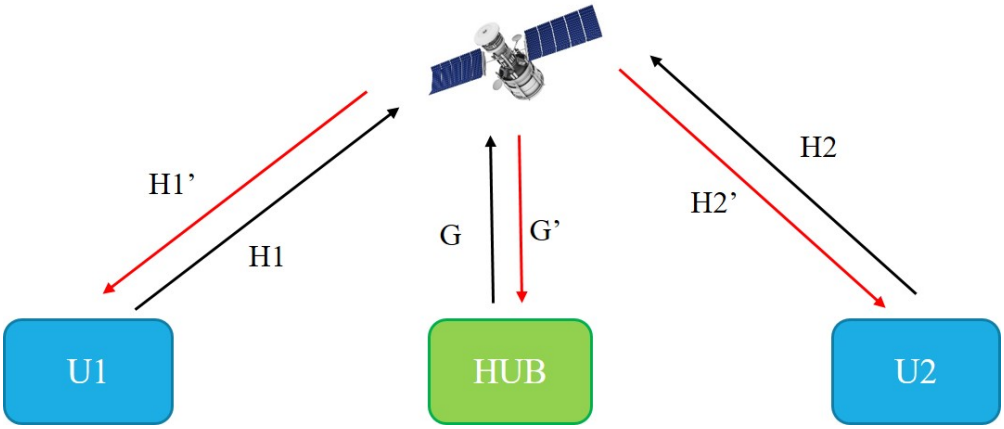

Figure 2.2: Two-phase Three-way Relay system

Similarly,

$$r_2 = H_2'.(s_1.H_1 + s_2.H_2 + s_G.H_G) + w = (H_2'.H_1.s_1) + (H_2'.H_2.s_2) + (H_2'.H_G.s_G) + w$$

At the hub,

$$r_G = H_G'.(s_1.H_1 + s_2.H_2 + s_G.H_G) + w = (H_G'.H_1.s_1) + (H_G'.H_2.s_2) + (H_G'.H_G.s_G) + w$$

2.2 ROLE OF CONSTELLATION SHAPING IN INTERFERENCE CHANNEL

In an interference channel with 2 different signals, we found out that if the gains of the signals are such that they add up orthogonally to each other, we get a better BER performance while decoding both the signals.

We also proved the gain-shaping ratio by running a MATLAB simulation for different gain ratios (or SIRs) and used joint-LLR method to decode them individually. This doesn't assume any super-constellation. Therefore, it can be proven that if the gains of the 2 signals are in the ratio 1:2, then they will add up orthogonally and the resultant super constellation will be a 16-QAM signal. This makes decoding more efficient.

Here, QPSK and 16QAM used are both unit-energy constellations.

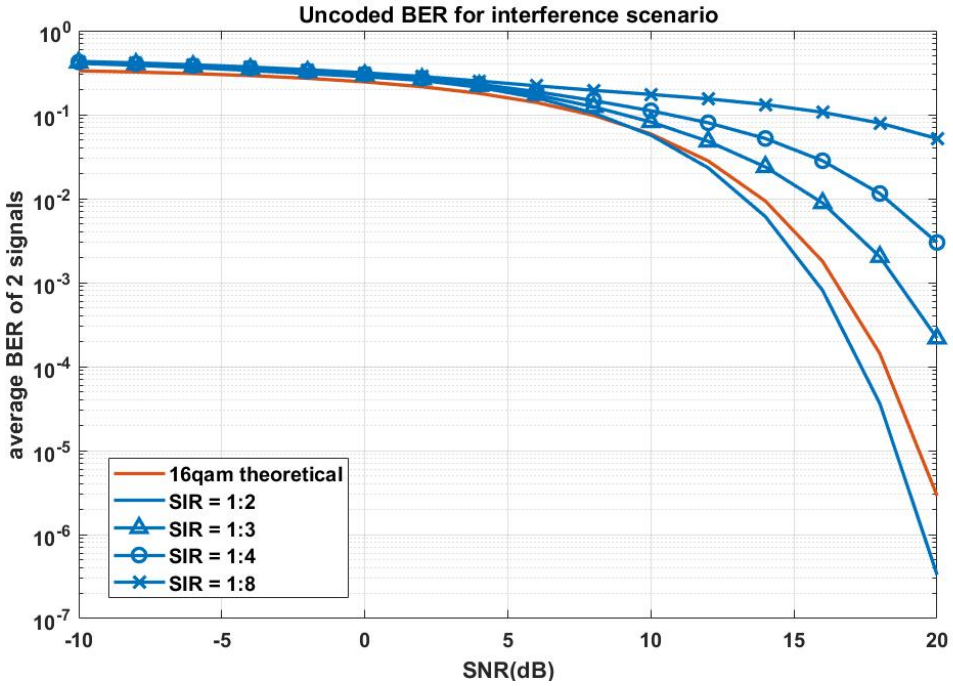

Figure 2.3: Average uncoded BER for different gain ratios

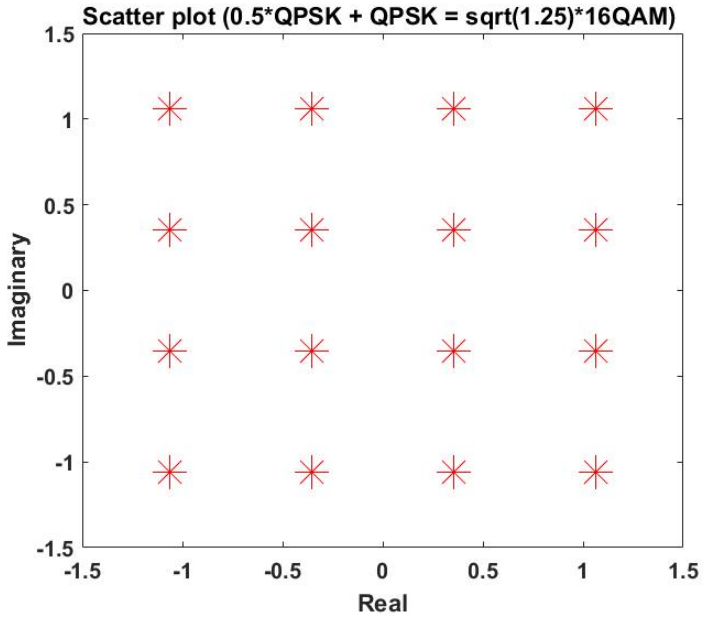

Figure 2.4: 0.5*QPSK + QPSK super-constellation

We use three different models: no interference model, interference model with ideal self cancellation and interference model with no ideal self cancellation.

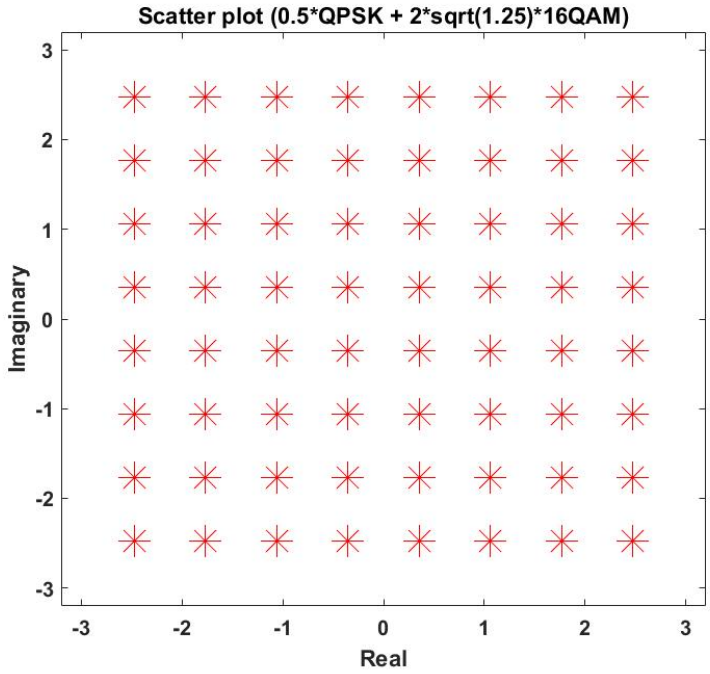

Figure 2.5: 0.5*QPSK + 2*$\sqrt{1.25}$*16QAM super-constellation

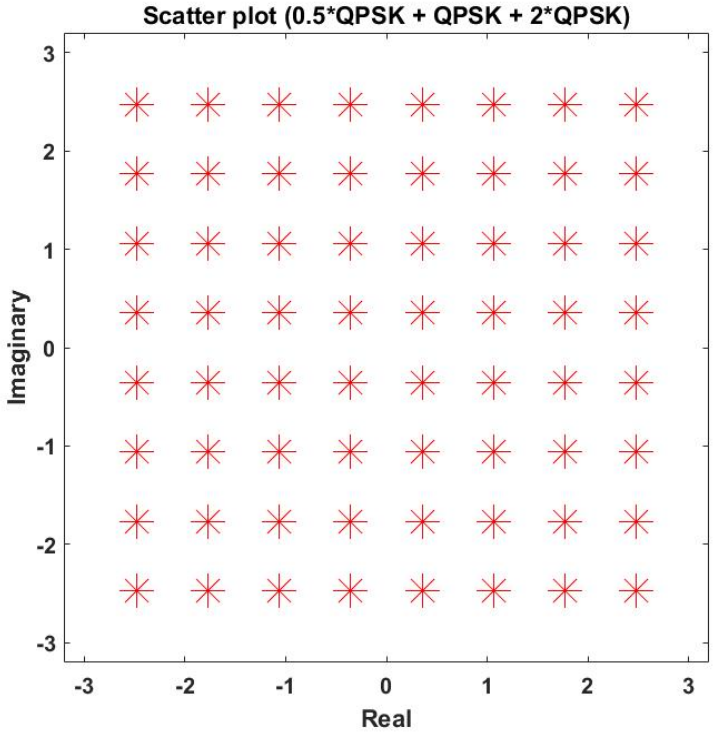

Figure 2.6: 0.5*QPSK + QPSK + 2*QPSK super-constellation

2.3 NO INTERFERENCE MODEL

In this model, only one of the users or hub can transmit a unit energy 16QAM symbol with gain of $\sqrt{1.25}$ in one block , while the other two only listen.

$$System{-}level\ throughput = N_{users}.N_{used-sc}.log_2(16).\frac{1}{2} = 4056\ bits\ per\ OFDM\ block$$

$$Power\ per\ user\ per\ block = \frac{1}{2}.(gain^2).N_{used-sc} = 633.75$$

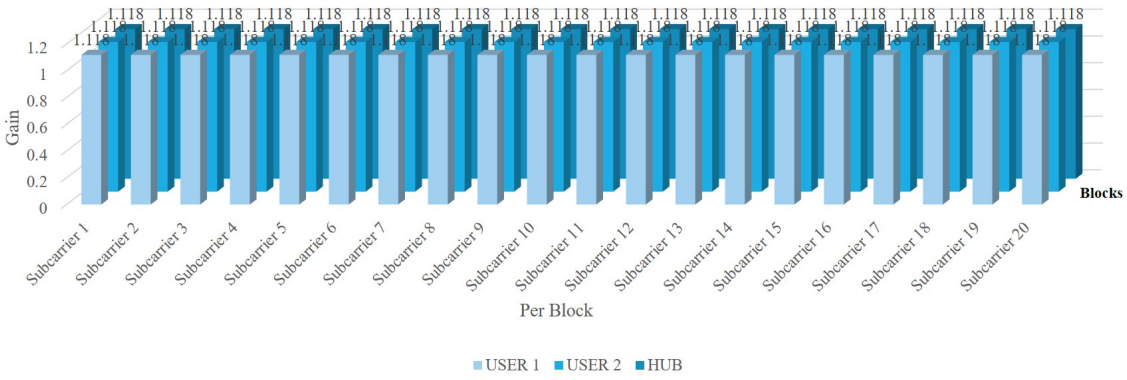

Figure 2.7: No interference scenario

2.4 INTERFERENCE MODEL

2.4.1 Joint-LLR approach for interference channel

Let,

$$y_G = (H'_G.H_1.s_1) + (H'_G.H_2.s_2) + w = H'_G.(H_1.s_1 + H_2.s_2) + w$$

Here, H_1 and H_2 are in the ratio 1:2 and s_1 and s_2 are orthogonal QPSK symbols.

To decode user 1,

$$\hat{s}_{1,k} = y_G - \alpha_1.q_{i,k} - \alpha_2.\{q_i\}$$

where, $\{q_i\}$ represents $(\pm\frac{1}{\sqrt{2}}, \pm\frac{1}{\sqrt{2}})$, k represents number of symbols in QPSK constellation and, α_1 and α_2 represents gain of user 1 and user 2 respectively.

Similarly, to decode user 2 information,

$$\hat{s}_{2,k} = y_G - \alpha_2.q_{i,k} - \alpha_2.\{q_i\}$$

These, $\hat{s}_1$ and $\hat{s}_2$ are used to calculate LLRs and sent to separate turbo decoders.

2.4.2 Decoding at Hub's end

After cancelling its own signal, the hub needs to decode only the users information,

$$y_G = (H'_G.H_1.s_1) + (H'_G.H_2.s_2) = H'_G.(H_1.s_1 + H_2.s_2)$$

To prove the effect of Constellation shaping on interference channel, both users send unit energy QPSK symbols in each sub-carrier of an OFDM block with alternate sub-carriers having higher gain for one of the users (gain ratio is 1:2).

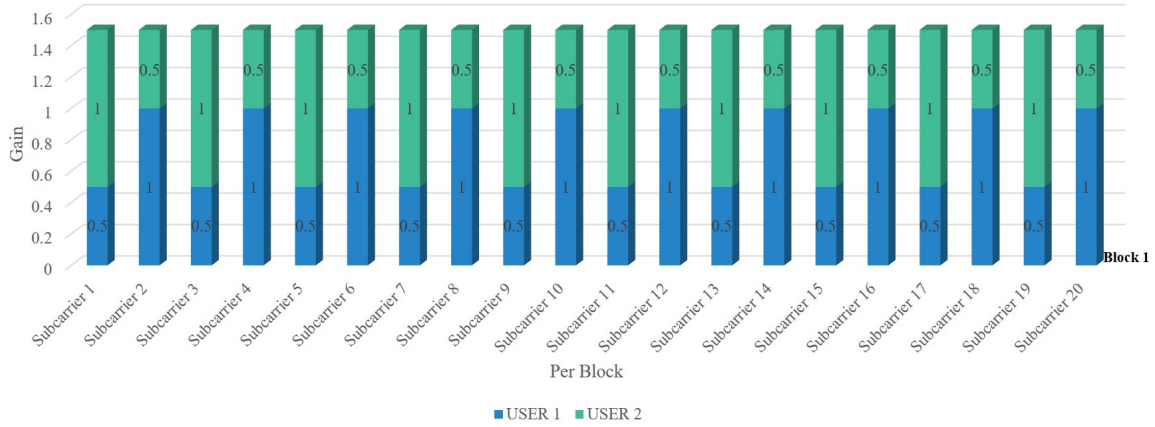

Figure 2.8: Signal received by hub after self-cancellation

In both the models, the system throughput as well as the energy spent per user per block remains the same.

$$System-level\ throughput = N_{users}.N_{used-sc}.log_2(4) = 4056\ bits\ per\ OFDM\ block$$

$$Power\ per\ user\ per\ block = \frac{1}{2}.\left((gain_1^2).N_{used-sc} + (gain_2^2).N_{used-sc}\right) = 633.75$$

The following are the system inputs for the simulation:

System Specifications	
Number of users	2
Number of blocks	10
Number of subcarriers	1024
Number of used-subcarriers	1014
Block length	672

Table 2.1: Relay system specifications

The average un-coded average BER of the two users is plotted.

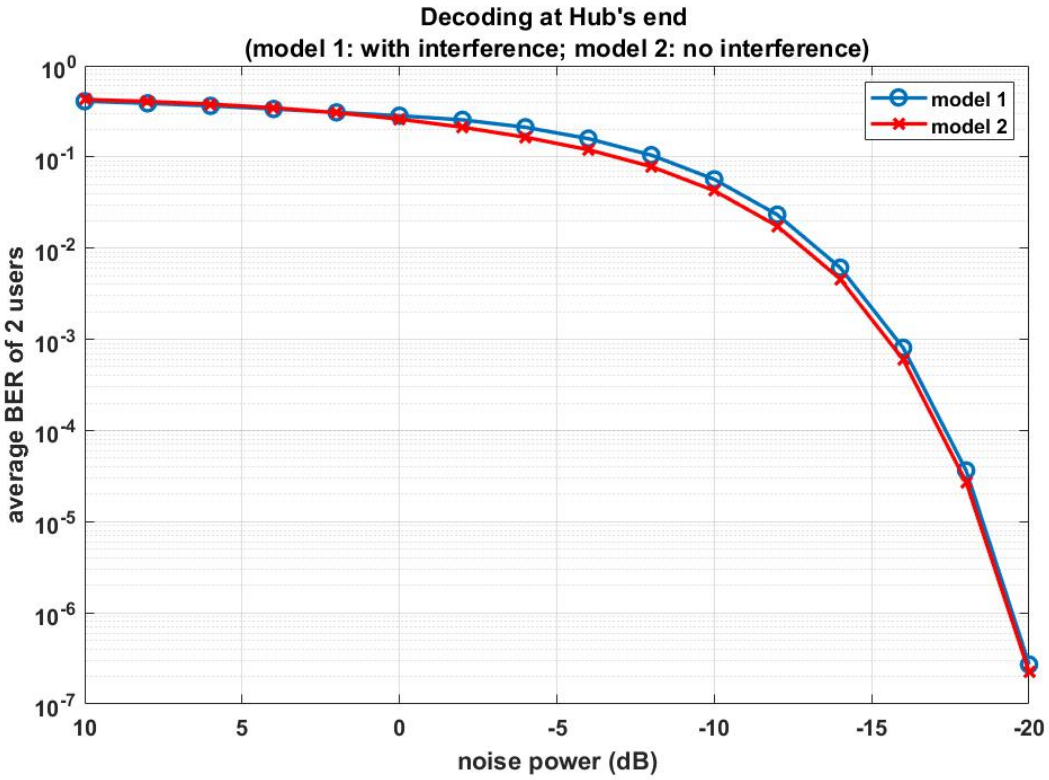

Figure 2.9: Uncoded average BER for model 1 and 2 at Hub's end

Observations

i. The uncoded BER for both models is quite close. As expected, joint-LLR performs works wonders in decoding the individual user signals even in an interference model.

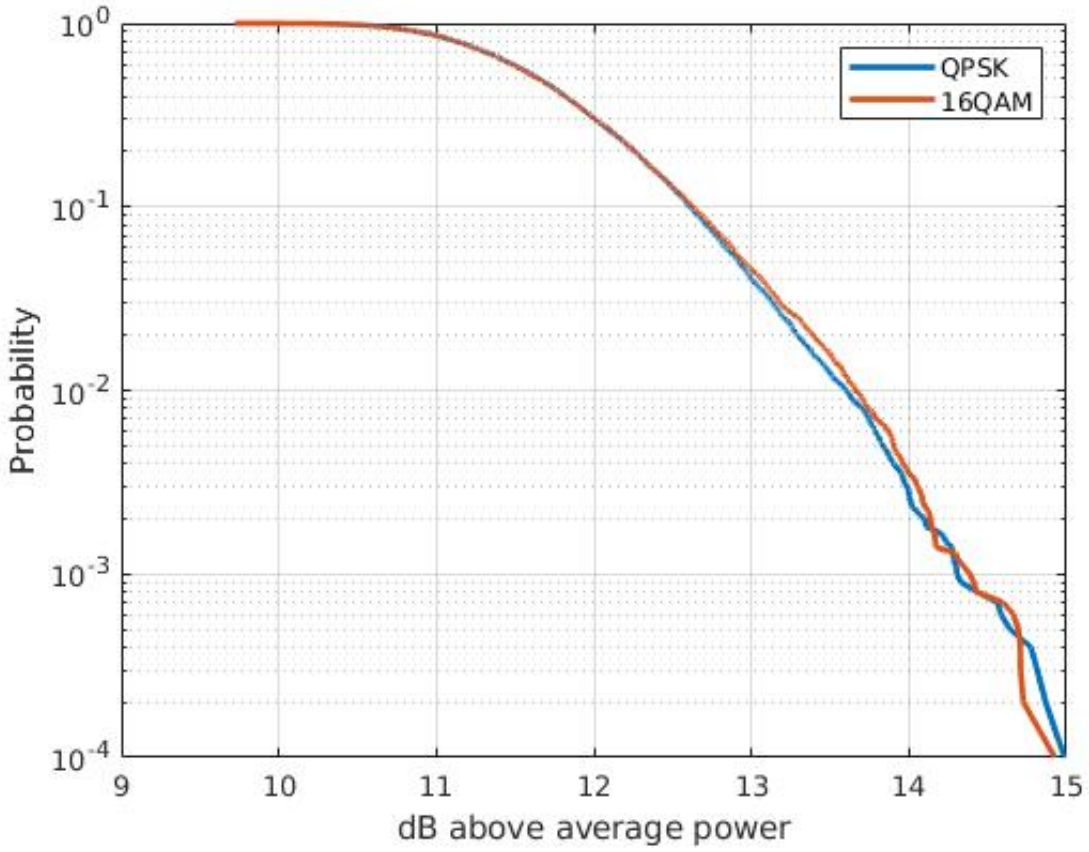

Figure 2.10: PAPR comparison when user sends QPSK vs 16QAM

ii. Both the scenarios showed equal Coded BER performance,as we have kept both the system level throughput and power per user per block to be the same.

iii. Even though no PAPR advantage is observed, the back-off is certainly lower in the case of QPSK as it is transmitting a lower modulation symbol. QPSK transmission is also more robust to the error vector magnitude.

With random phase error

Apart from AWGN noise, we also include a random phase error in the channel. This phase error is estimated and corrected for at the receiver. The average coded and un-coded BER of the two users is plotted for the same two scenarios.

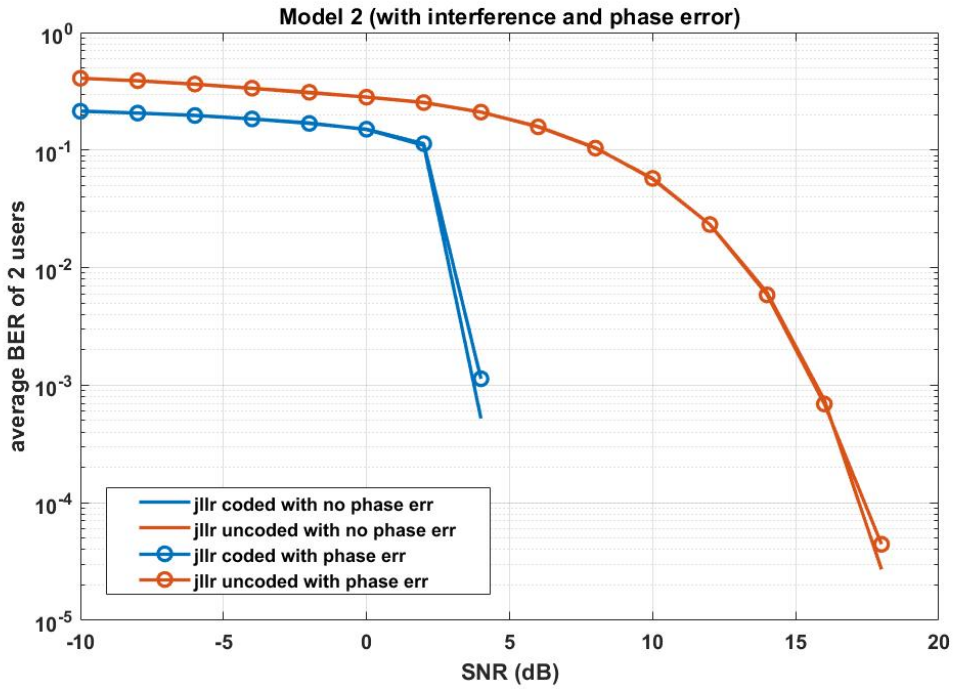

Figure 2.11: Coded and Uncoded BER for Model 2 with random phase error

Observations

i. Even with random phase error case, joint-LLR and constellation shaping are together helping us achieve a good BER. Both coded and uncoded BER with and without random phase error is comparable with no-phase error plots having slightly better performance.

ii. The better the phase error estimate, the closer the plots will be to the ideal no-phase error case.

2.4.3 Decoding at UE's end

After the UE cancels its own signal, it is left with the other UE's signal and the Hub's signal to decode.

Here, we propose three solutions based on the application:

1. In the first solution, both the UEs are precoded in 1:2 gain ratio with each of them transmitting only a QPSK signal (as before). Hub also sends QPSK signal at a lower gain (of 0.5) but by repeating the same information for two consecutive subcarriers.

2. In the second solution, both the UEs are precoded in 1:2 gain ratio with each of them transmitting only a QPSK signal (as before). Hub now sends QPSK signal at a higher gain (of 1) again by repeating the same information for two consecutive subcarriers.

3. In this solution too, both the UEs are precoded in 1:2 gain ratio with each of them transmitting only a QPSK signal (as before) but the Hub now sends a 16QAM signal with still repeating the same information for two consecutive subcarriers.

In the first 2 solutions, the system level throughput and power of each user per block is kept equal for better comparison. But if the hub wishes to increase its throughput, without changing the power of each user, solution 3 can be used.

The UE first decodes the information of other UE and Hub on sub-carriers where constellation shaping is ensured, and then uses the decoded Hub's information to cancel it from the remaining sub-carriers of the other UE.

For example, with respect to UE2:

$$y_2[2k] = (H_2'.H_1.s_1[2k]) + (H_2'.H_G.s_G[2k]) = H_2'.(H_1.s_1[2k] + H_G.s_G[2k])$$

Joint-LLR is performed to decode hub's signal and UE_1 signal on even sub-carriers.

On the odd sub-carriers,

$$y_2[2k+1] = (H_2'.H_1.s_1[2k+1]) + (H_2'.H_G.s_G[2k])$$

After subtracting the Hub's signal,

$$y_2[2k+1] - (H_2'.H_G.s_G[2k]) = H_2'.H_1.s_1[2k+1]$$

Normal LLR is used to decode the UE_1 signal on odd sub-carriers.

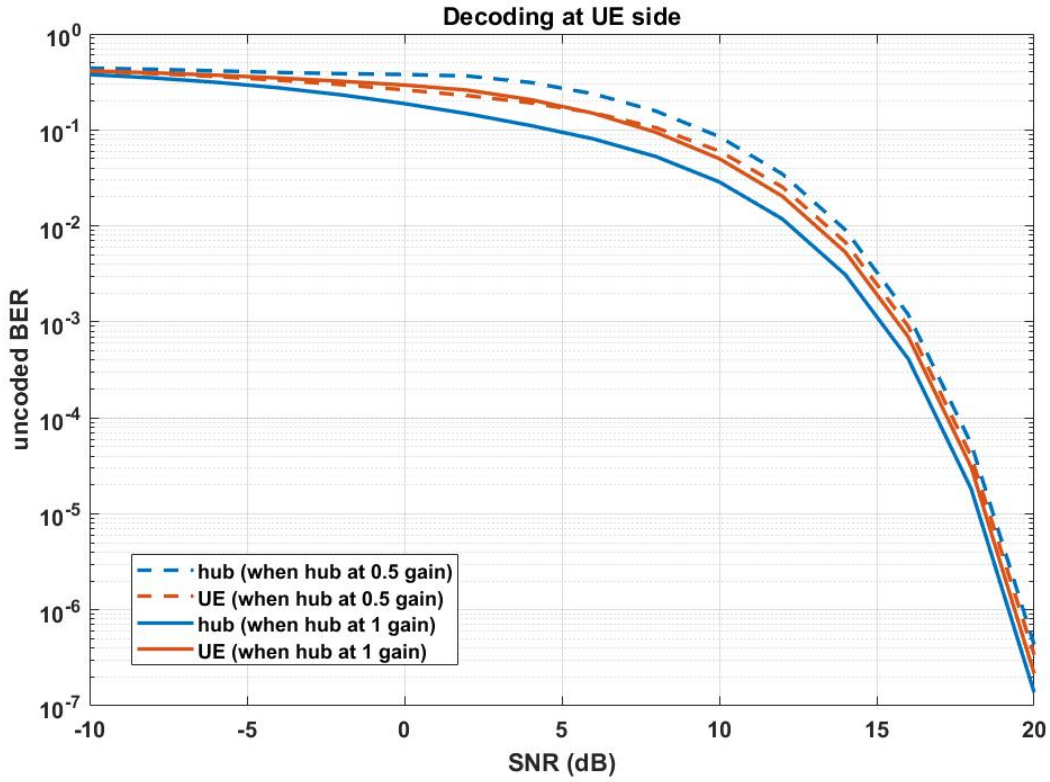

Figure 2.12: Average BER of UE and hub for QPSK with gain 0.5 and gain 1

Observations

- In the second solution when hub sends its QPSK signal with gain 1, the hub's and other UE's signal are both decoded better at the even sub-carriers. Therefore, when this estimate is subtracted from the odd subcarriers of the other UE's signal, even that is decoded better and overall performance is better.

In solution 3, the hub repeats itself for 2 consecutive subcarriers and it sends unit energy 16QAM symbols with a gain of $2 * \sqrt{1.25}$. Here, 64QAM super-constellation is used.

Similar process is followed that in alternate subcarriers where constellation shaping is ensured, joint LLR is used to decode and then this hub signal is cancelled from the other

set of subcarriers and decoded.

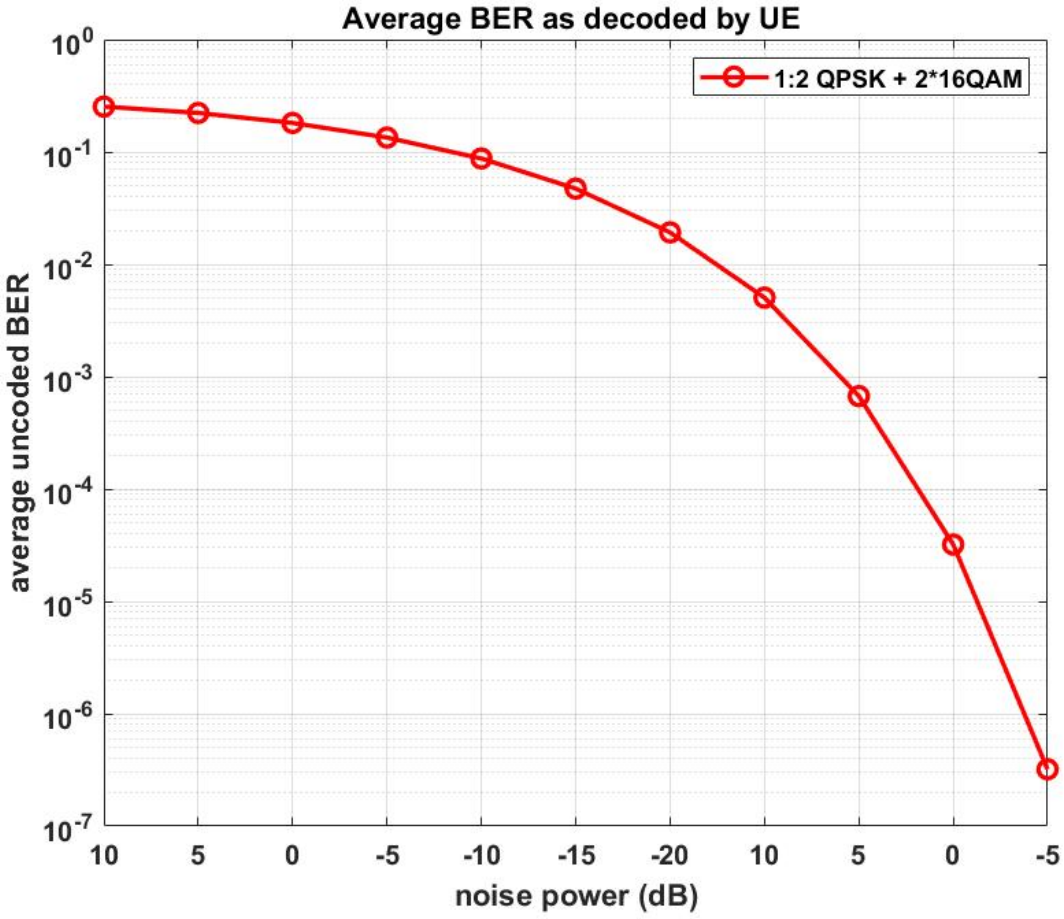

Figure 2.13: Average BER of UE and Hub as decoded by the other UE

2.5 SIMULTANEOUS JOINT-LLR WITH NO IDEAL SELF CANCELLATION

In this application of the relay system, we do not assume ideal self-cancellation at any end. The precoding is done such that all the receivers (both the UEs and the hub) decode all signals and use only what it needs. In the first solution, both the UEs and hub are

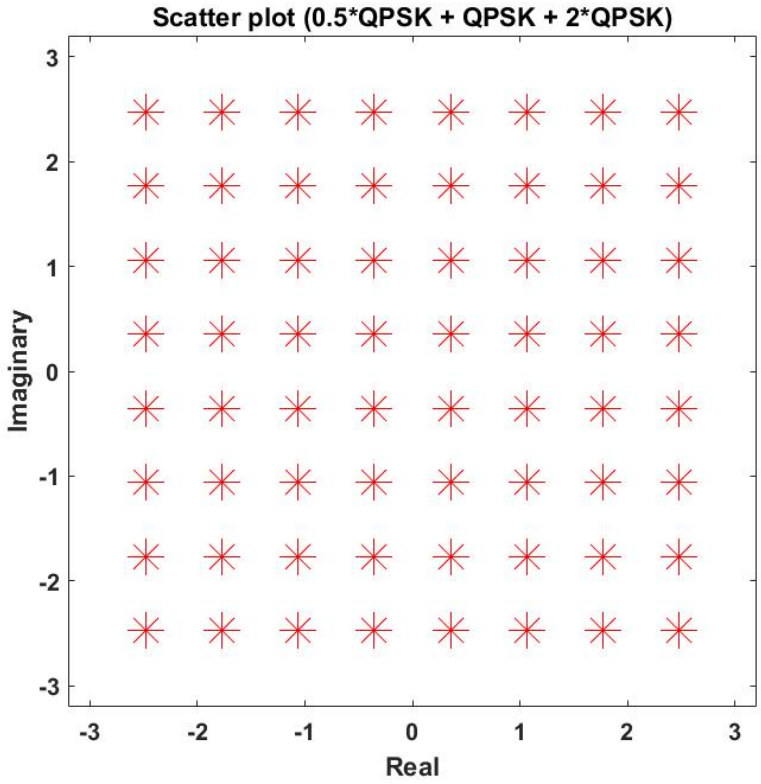

Figure 2.14: 64QAM Super-constellation formed from 3 QPSK signals

precoded in 1:2:4 gain ratio with each of them transmitting only a unit energy QPSK signal. Simultaneous joint-LLR is done at each of those nodes to decode all three signals. The constellation shaping property is still used but to form a 64QAM super-constellation.

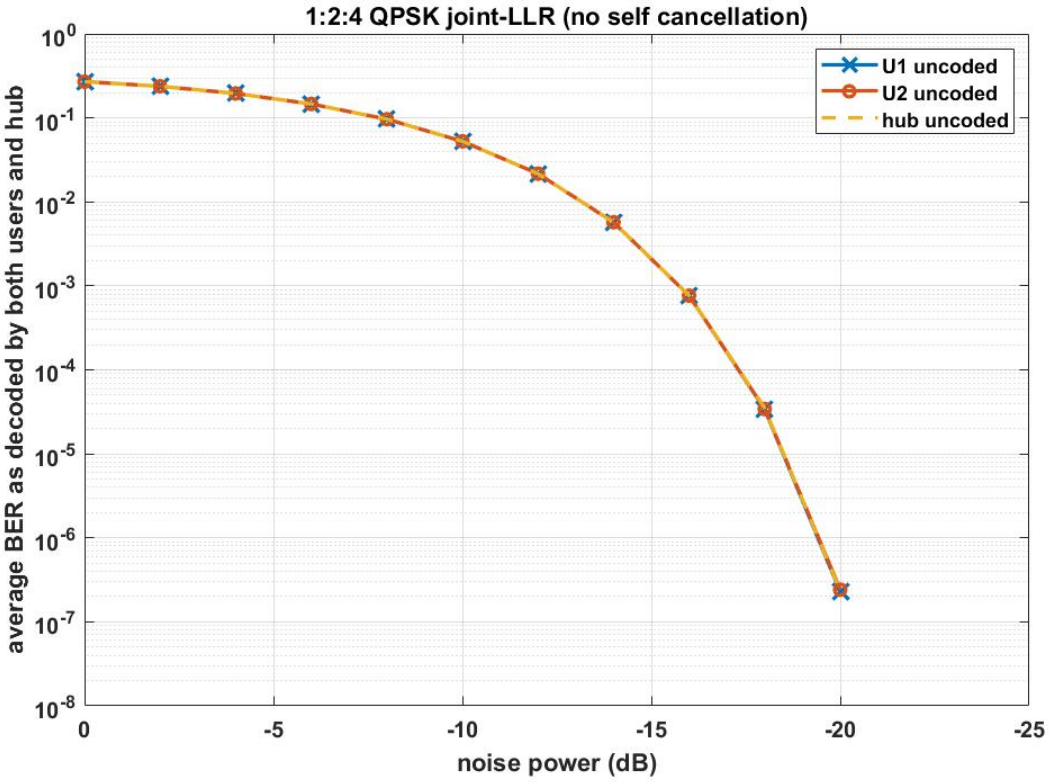

Figure 2.15: Simultaneous decoding of all three signals

2.6 FINAL COMPARISON

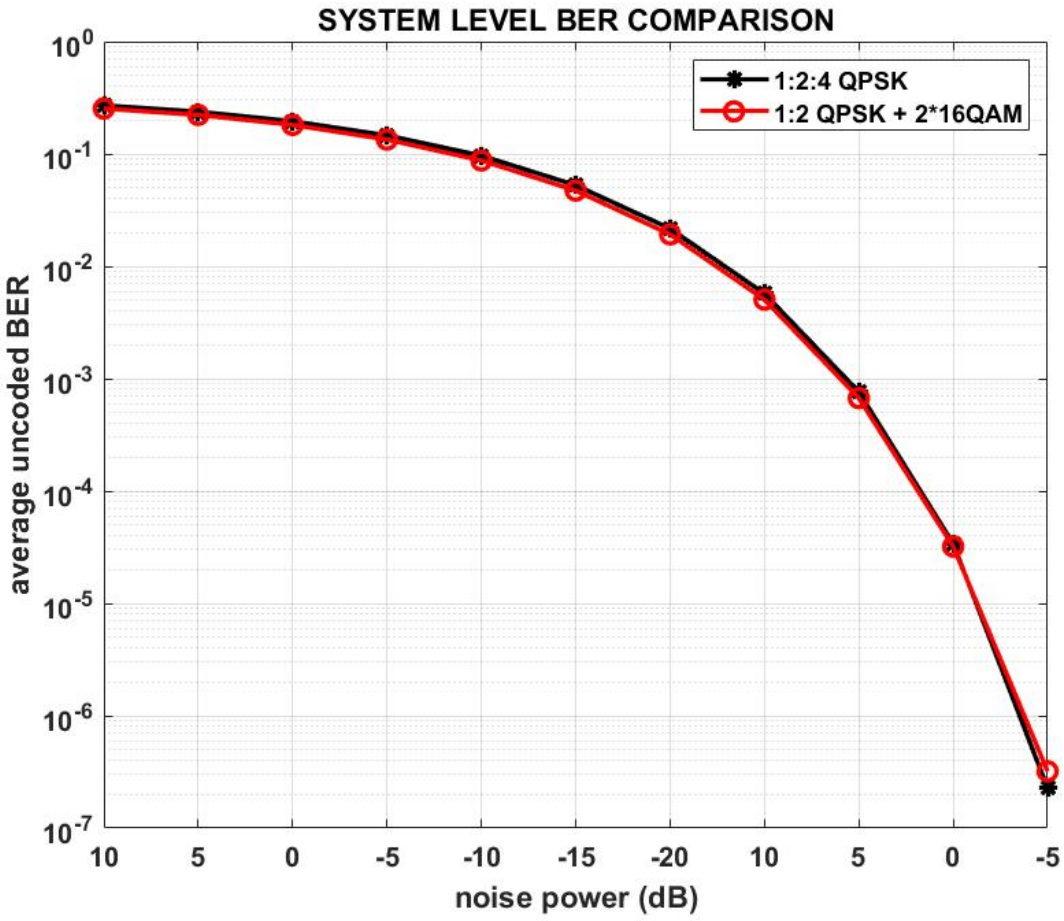

Figure 2.16: Interference model comparison with and without self-cancellation

Observations

i. The simultaneous joint-LLR model with no ideal self cancellation performs as well as the interference model with hub repeating itself but with a $2 * \sqrt{1.25}$ unit energy 16QAM signal.

ii. This is achieved at no extra cost. The users are still transmitting at the same power and the throughput of each of the users and hub is still the same.

iii. Compared to the No interference model when only one of the users/hub is transmitting, the spectral efficiency in the no ideal self-cancellation model is almost 4.5 times more.

iv. The spectral efficiency in the no ideal self-cancellation model is the same as the

with self-cancellation model with hub repeating itself but with a $2 * \sqrt{1.25}$ unit energy 16QAM signal

TRANSMITTED			SPECTRAL EFFICIENCY @ SATELLITE END	
UE1	**UE2**	**HUB**		
$\sqrt{1.25}$ *16QAM	-	-	(4 bits/ subcarrier)/ 3 OFDM blocks	**NO INTERFERENCE**
0.5*QPSK	1*QPSK	0.5*QPSK	(10 bits/ 2subcarriers)/ 1 OFDM block	**WITH IDEAL SELF-CANCELLATION**
0.5*QPSK	1*QPSK	1*QPSK	(10 bits/ 2subcarriers)/ 1 OFDM block	
0.5*QPSK	1*QPSK	2*$\sqrt{1.25}$ *16QAM	(12 bits/ 2subcarriers)/ 1 OFDM block	
0.5*QPSK	1*QPSK	2*QPSK	(6 bits/ 1subcarriers)/ 1 OFDM block	**WITHOUT IDEAL SELF CANCELLATION**

Figure 2.17: Improvement in Spectral Efficiency

2.7 EXTENSION TO N-WAY RELAY SYSTEM

This constellation shaping can be used to extend our system to an N-way relay with a higher modulation super-constellation along with joint-LLR computation to make decoding easier. However, as more users add up and a bigger super-constellation is formed, even the theoretical BER performance will depreciate. Instead, sets of sub-carriers can be are allotted for different UEs to communicate.

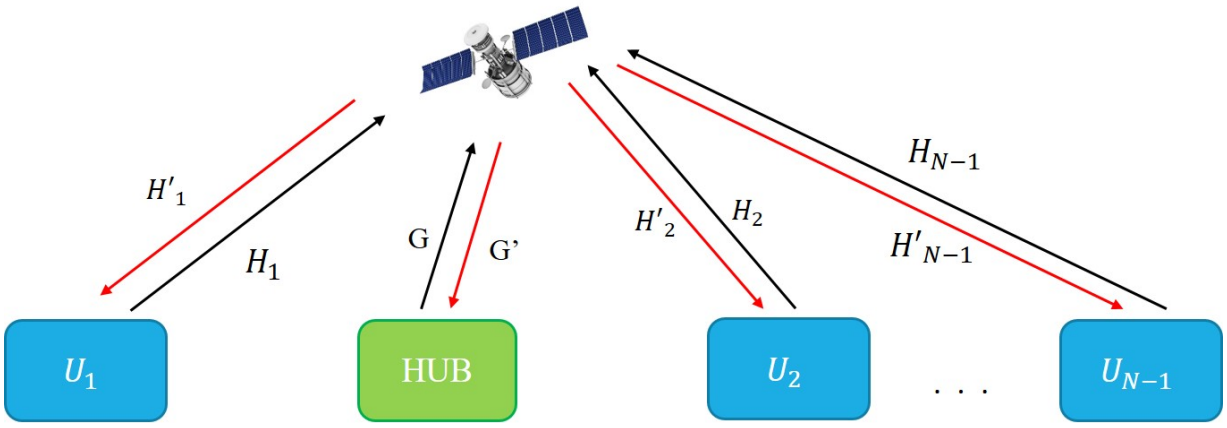

Figure 2.18: Two-phase N-way Relay

CHAPTER 3

RELIABLE AND COVERT SATELLITE COMMUNICATION SYSTEM

3.1 INTRODUCTION

Satellite Communication is essential in strategic applications and the requirement of reliable covert satellite communication is vital in the present security scenario. The objective of the project is to design a satellite communication air interface which can provide robust communication with minimum probability of detection and interception with moderate complexity with respect to hardware and algorithms. This work combines different techniques like single carrier block modulated DS CDMA and Interleaved OFDM for orthogonal multiple access. RCS forward link is point to multi-point communication via Satellite between the central Hub and user equipment present across the length and breadth of our country, and the RCS reverse link is a multi-point to point communication system.

The objective of the project work is to design a satellite air interface for a full duplex communication between a central hub and 32 users (UEs) via a geostationary satellite (approx. 36500 km from earth) across a geographical area expanse over the whole country having following features:

i. Low probability of interception and low probability of detection (LPD/LPI)

ii. High Reliability

iii. Low Peak to Average Power Ratio, manageable within the constraints of the satellite specification

iv. User support data rate of 4kbps within the available 36 MHz bandwidth

Forward link – The Hub will be transmitting over f_1' and UE will be receiving over f_2.

Reverse link – The UE will be transmitting over f_1 and Hub will be receiving over f_2'.

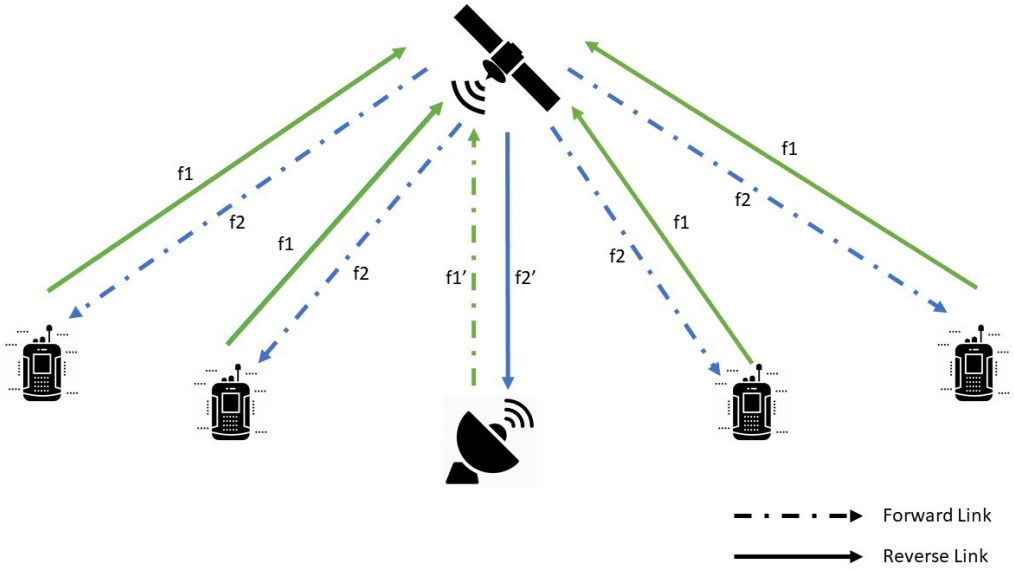

Figure 3.1: RCS FDD layout

The FDD layout for RCS is as shown. FDD setup will require the Hub and User Equipment to operate over two different carrier frequencies using a duplexer setup. f_1 and f_1' being carrier frequency separated by 18 MHz and f_2 and f_2' being another set of carrier frequencies separated by 18 MHz. The channel bandwidth for f_1 and f_1' will be 17.875 MHz each separated by a 250 kHz guard band; with same specification for f_2 and f_2'.

To provide covertness to the system, the pre-processing SNR observed at the intended receiver (and hence, in at eavesdropper) is very low, and nearly 15dB below the thermal noise floor. Direct sequence type spreading, narrow banding, information repetition, and FEC were employed in tandem to give a total post-processing gain of nearly of 39.12dB. This ensures tremendous reliability and a healthy fade-margin (excess link margin) of more than 18dB, which provides >99% uptime even in the presence of Rician fading.

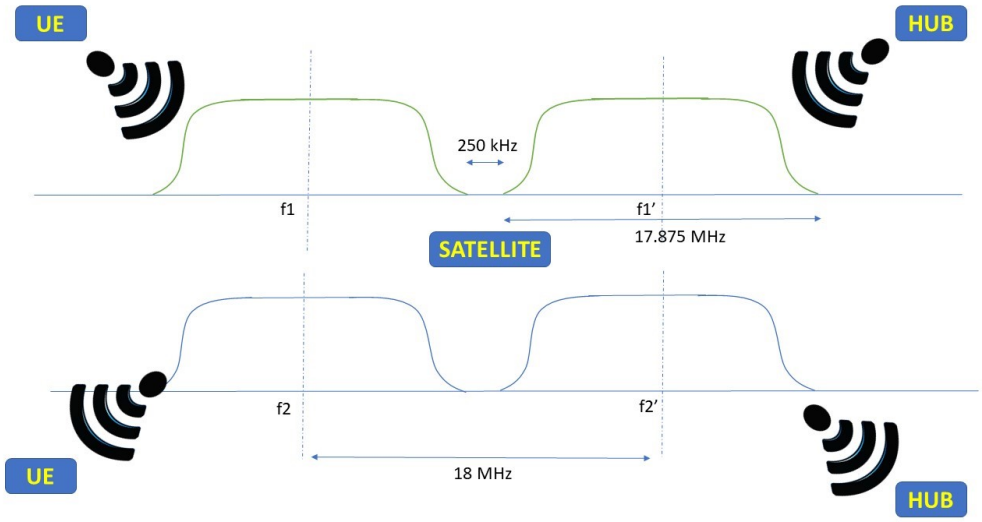

Figure 3.2: RCS FDD layout

3.2 FORWARD LINK OVERVIEW

3.2.1 FL: Transmitter block

i. Forward link FDD, uses single carrier DS CDMA with block modulation to achieve low probability of detection and interception.

ii. The Hub supports a data rate of 4 kbps for each UE over the forward link of 1000 ms duration.

iii. The data from Hub for a single UE will be encoded by the Forward error correction block (turbo encoder of rate ...) to provide 5.4 kbps data rate at the output.

iv. The data stream will then be spread using orthogonal Walsh Hadamard code sequences by a factor of 2048 followed by mapping to QPSK symbols and separated into orthogonal I and Q streams.

v. The spread sequence will then be block modulated as per the framing structure and pulse shaped (Raised cosine window) to provide 15,625,000 chips over 1 sec forward link frame, which will then be converted to analog form, mapped onto the carrier and transmitted.

vi. The Hub will have 32 FL transmitter UE blocks as shown in figure. The signals from each of these blocks will be added before DAC. Summation, DAC and carrier mapping block will be common to all the UEs.

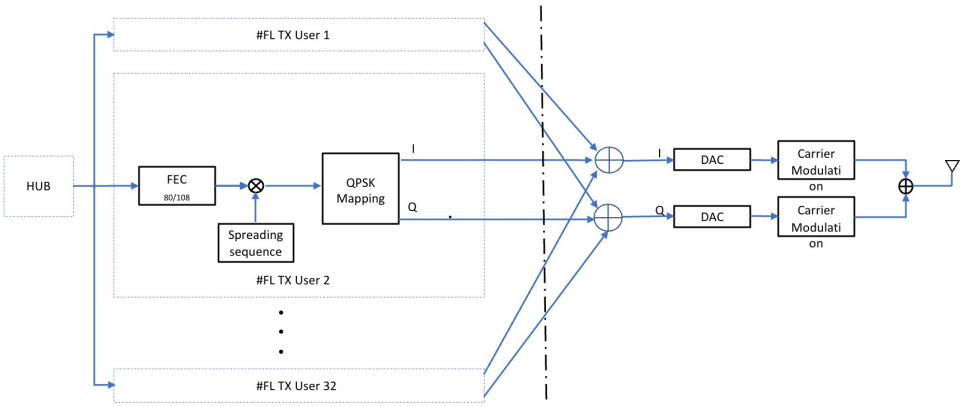

Figure 3.3: FL Transmitter block

3.2.2 FL: Receiver block

i. For every frame, the received signal will be processed for determining the frequency offset and timing recovery using hypothesis testing from the preamble of the received framed implemented through correlated banks. Corresponding frequency offset correction will be applied along with timing boundary knowledge to the following received symbols.

ii. For every subframe, received pilot symbols for channel estimation are coherently added to boost the SNR and then the channel frequency response will be estimated with knowledge of transmitted Zadoff Chou pilot symbols using frequency domain estimation. Accordingly, all received data symbols are equalized using the channel estimate from pilots through zero forcing followed by the de-spreading operation. The de-spreading sequence will be unique to every UE.

iii. The de-spreaded symbol will be delayed and then soft combined with the subsequent symbol to obtain a coherent averaging gain.

iv. The soft combining will be followed by QPSK demodulation and error correction using Turbo codes.

3.3 REVERSE LINK OVERVIEW

3.3.1 RL: Transmitter block

i. Reverse link works on spread interleaved OFDMA(SI-OFDMA) with differential QPSK modulation.

ii. In reverse link, every chip (data, pilot, PRACH) transmitting by UE must be sent

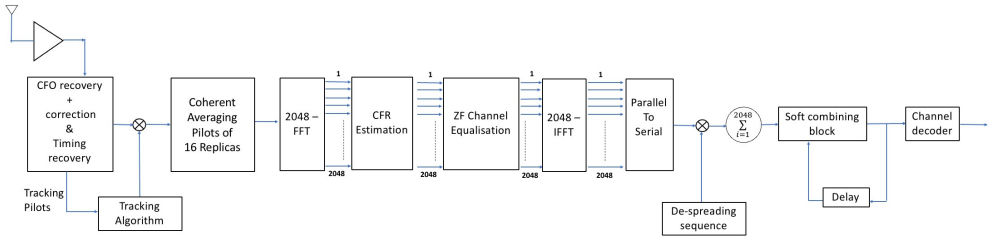

Figure 3.4: FL Receiver block

after frequency compensation (shown as θ_i for i^{th} UE) estimated through forward link. This is unlike forward link because reverse link scenario is a multi-point to point where multiple UEs transmit at the same time and each user's data has different frequency offset error, which is difficult to handle at hub's side.

iii. Like Forward Link, Reverse link also supports a data rate of 4 kbps for each UE.

iv. Each UE's data is encoded by the Forward error correction block (turbo encoder of rate $\frac{1}{2}$ or $\frac{2}{3}$) to provide a coding gain.

v. In order to optimize the PAPR problem at satellite end, pilot design has been customized based on the number of UEs in the network. A lookup table has been formed which helps an UE to choose pilot QPSK symbols depending on the number of UEs already connected to the network. This scheme will make sure the overall PAPR in all the cases where number of UEs varying until 32 has been kept low, which leaves us room for boosting CCE at UE end.

vi. The encoded data stream will be mapped to differentially modulated QPSK symbols and separated into orthogonal I and Q stream.

vii. The data symbol streams first will be spread by best possible Zadoff-Chu sequence of 64 length (in terms of overall PAPR) and repeat each spread block 32 times to accommodate 32 UEs followed by appropriate comb allocation at every UE.

viii. To this data, CP is added and then pulse shaped (Raised cosine window) SI-OFDMA is used as per the framing structure and which will then be converted to analog form, mapped onto the carrier and transmitted.

3.3.2 RL: Receiver block

i. Timing synchronization involves cross correlation with all the assigned Zadoff-Chu sequences for existing UEs in the network. This ensures that all the UEs have been ranged such a way that relative delay between first and last arriving uplink signal is less than cyclic prefix.

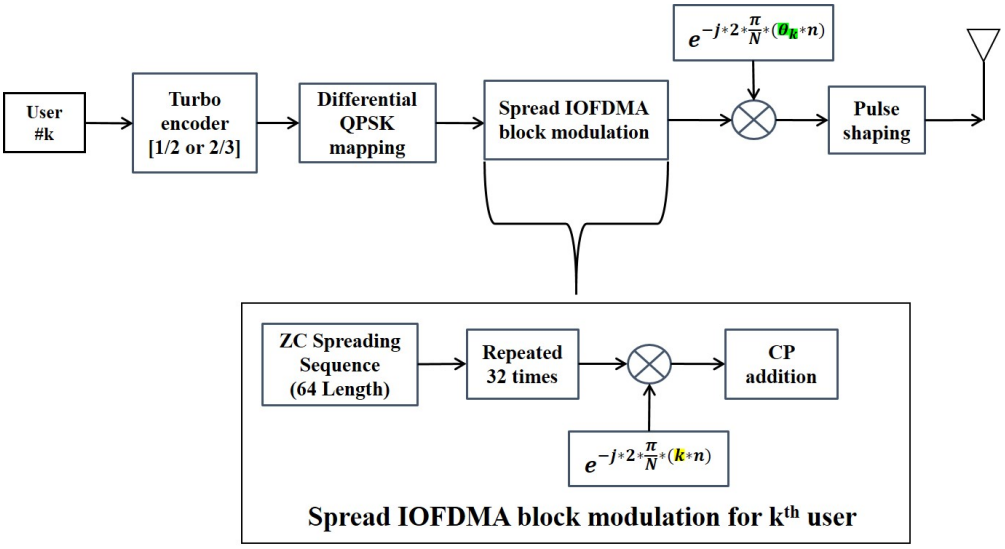

Figure 3.5: RL Transmitter block

ii. According to first and last peak from cross-correlation of Zadoff-Chu (ZC) we can choose IBI free FFT window.

iii. At the start of every subframe, channel frequency response (CFR) estimation for every UE to Hub link is done by coherently adding 64 copies of received pilot symbols to boost SNR and then followed by FFT. Then, each UE's received comb has been separated and multiplied by conjugate of UE-specific transmitted pilot fetch us CFR of each UE. This estimated CFR also captures the additional phase error caused due to shift in FFT window from critical boundary.

iv. After taking FFT, every UE's data symbol is equalized (ZFE) using every UE's respective estimated CFR.

v. After zero-forcing equalization (ZFE) for all UEs, interleave every UE's equalized frequency response with 32 zeros and assign it to 1st UE's comb index to avoid any frequency shift at the end and then take IFFT. This will in turn gives 15 dB gain as every UE occupies 1⁄32 portion of whole bandwidth. DOUBT!!!!!

vi. After zero-forcing equalization (ZFE) for all UEs, perform a 64-point IFFT and de-spread with transmitted ZC.

vii. After pre-processing, bit-level LLRs are generated and passed to the Turbo decoder.

RL Design Highlights

- Comb Selection Rule depends upon number of active users for minimising overall PAPR (data region)

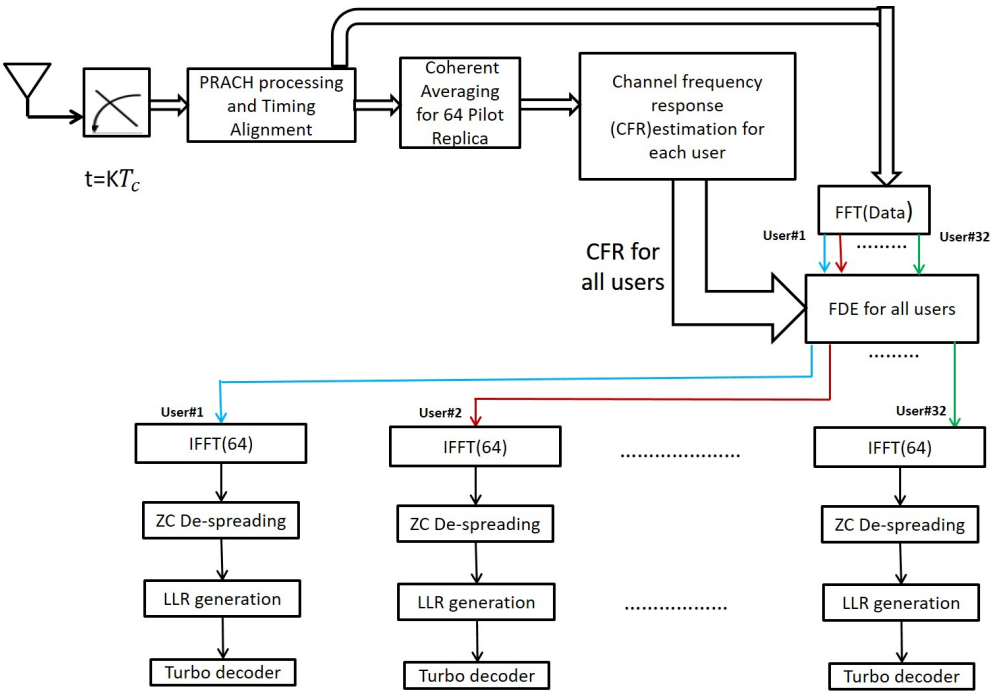

Figure 3.6: RL Receiver block

- Lookup table of QPSK pilot symbols depends upon number of active users for minimising overall PAPR (pilot region)
- Choosing Spreading sequence as Zadoff-chu instead of Walsh code to exploit frequency diversity
- Using TCC instead of MPCC has helped us avoid the repetition of data twice at the receiver end of RL

3.3.3 RL Frame Structure while using Turbo codes

To avoid the repetition of data twice, the requirements of the project changed to using Turbo codes as the FEC instead of MPCC.

Frame structure description for half code rate

i. In the reverse link design, every UE will transmit 4,288 different DQPSK symbols (16 subframes X 268 complex data symbols).

ii. The chip duration is 0.0651 μseconds

iii. The PRACH structure will have 4,60,800 chips, which corresponds to 30 ms,

followed by periodic ranging where 4096 chips duration of ZC sequence repeated twice for each UE.

iv. Each sub-frame makes up for 8,66,688 chips corresponding to 56.4ms, out of which 1,31,200 chips (8.5 ms) are dedicated for CCE.

v. Followed by CCE, are 2 code blocks with 134 SI-OFDM symbols each of 2,176 chips. 70 dummy symbols follow the two code blocks.

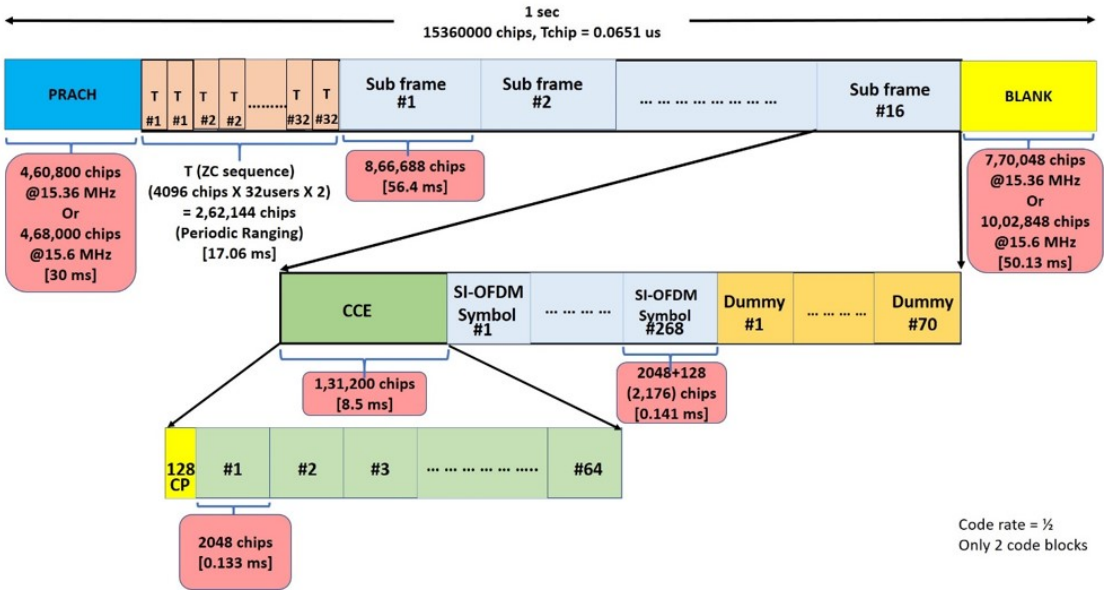

Figure 3.7: RL Frame structure for 1/2 code rate

Frame structure description for two-third code rate

i. In the reverse link design, every UE will transmit 4,896 different DQPSK symbols (16 subframes X 306 complex data symbols).

ii. The chip duration is 0.0651 μseconds

iii. The PRACH structure will have 4,60,800 chips, which corresponds to 30 ms, followed by periodic ranging where 4096 chips duration of ZC sequence repeated twice for each UE.

iv. Each sub-frame makes up for 8,66,688 chips corresponding to 56.4ms, out of which 1,31,200 chips (8.5 ms) are dedicated for CCE.

v. Followed by CCE, are 3 code blocks with 103 SI-OFDM symbols each of 2,176 chips. 32 dummy symbols follow the two code blocks.

vi. Although more symbols are being transmitted in 2/3 code rate, we notice that the

performance is better for 1/2 code rate.

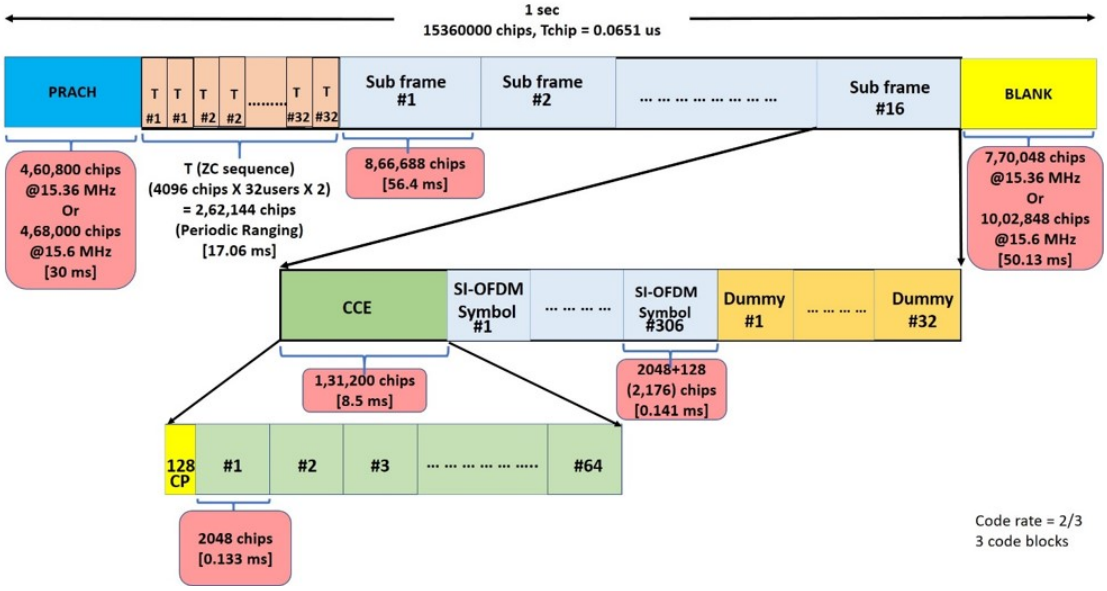

Figure 3.8: RL Frame structure for 2/3 code rate

CHAPTER 4

SIMULATION RESULTS FOR RCS

4.1 SYSTEM MODEL

The following are the system inputs for the simulation:

System Specification in RL	
Chip duration	0.0651μseconds
Number of users	32
Number of blocks Number of blocks	2 (for rate $\frac{1}{2}$) 3 (for rate $\frac{2}{3}$)
Number of subcarriers	2048
Block length	128
Number of symbols Number of symbols	134 (for rate $\frac{1}{2}$) 103 (for rate $\frac{2}{3}$)
Cyclic Prefix length	128
Zadoff-Chu sequence	64
FFT size	64

Table 4.1: RCS simulation system specifications

At the Reverse link, three signal impairments have been introduced apart from noise.

$$y[n] = \sum_{p=1}^{N_{users}} \alpha_p x_p[n - \delta_p] e^{-j.2\pi n \frac{\Delta f_p}{f_s}} + w[n]$$

where,

$y[n]$ aree received samples at hub,

$x_p[n]$ are the transmitted IFDMA samples from p^{th} user,

$w[n] \approx AWGN$ with variance σ^2

N_{user} is the number of users in the system,

α_p is relative power difference among user data,

δ_p is relative timing offset across user data

Δf_p is residual CFO error for every user data

4.2 SCENARIO 1

i. Power parameter, $\alpha_p = 1$ for all users

ii. Residual CFO, $\Delta f_p = 0$ for all users

iii. Timing offset δ_p modelled as discrete random variable sampled from $U\{0, N_{CP}\}$ Assuming every user has been ranged such that first and last arriving user frame boundary offset is less than or equal to 128 chips.

4.2.1 Results

Average BER and BLER are plotted.

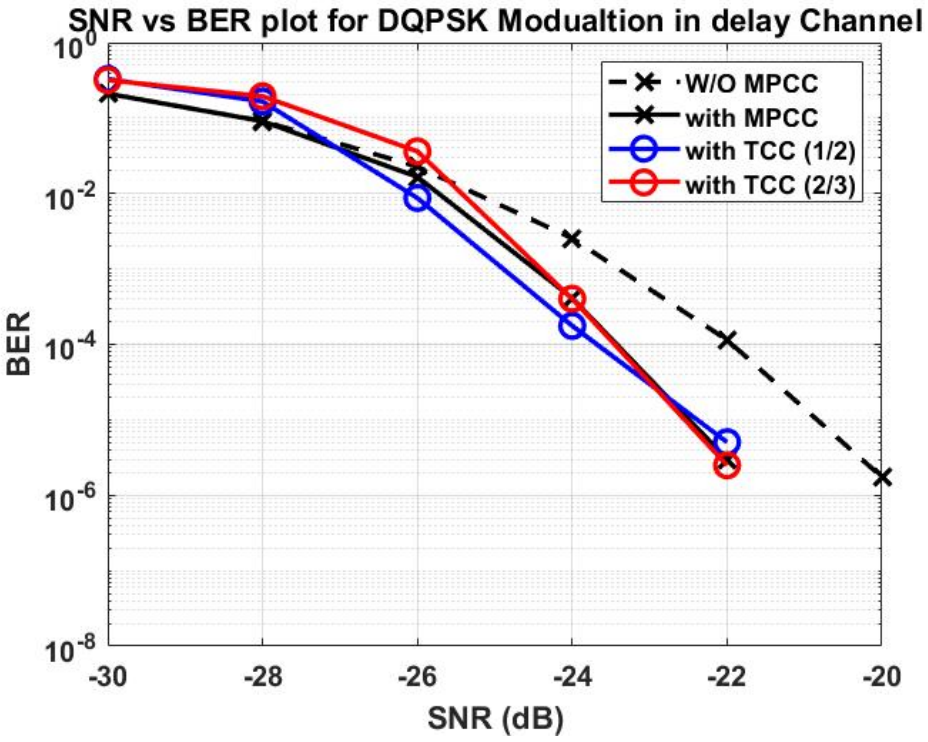

Figure 4.1: Average BER for Scenario 1

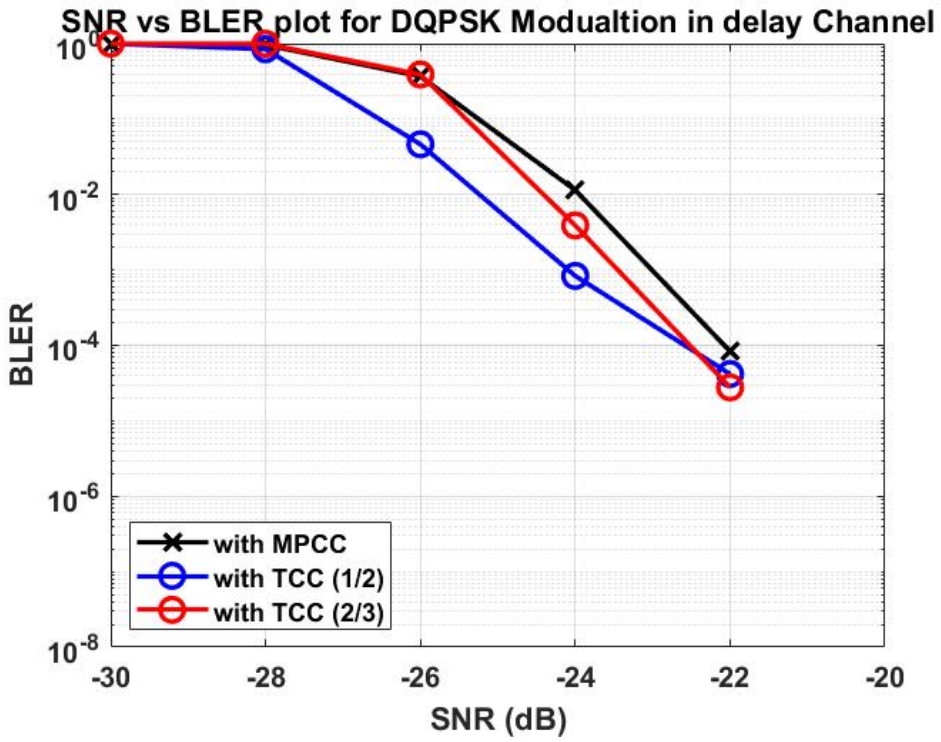

Figure 4.2: Average BLER for Scenario 1

4.3 SCENARIO 2

i. Power parameter, $\alpha_p = 1$ for all users

ii. Residual CFO, Δf_p modelled as discrete random variable sampled from $U\{-\Delta f_{max}, \Delta f_{max}\}$

iii. Timing offset δ_p modelled as discrete random variable sampled from $U\{0, N_{CP}\}$

4.3.1 Results

Average BER and BLER are plotted.

For rate $\frac{1}{2}$:

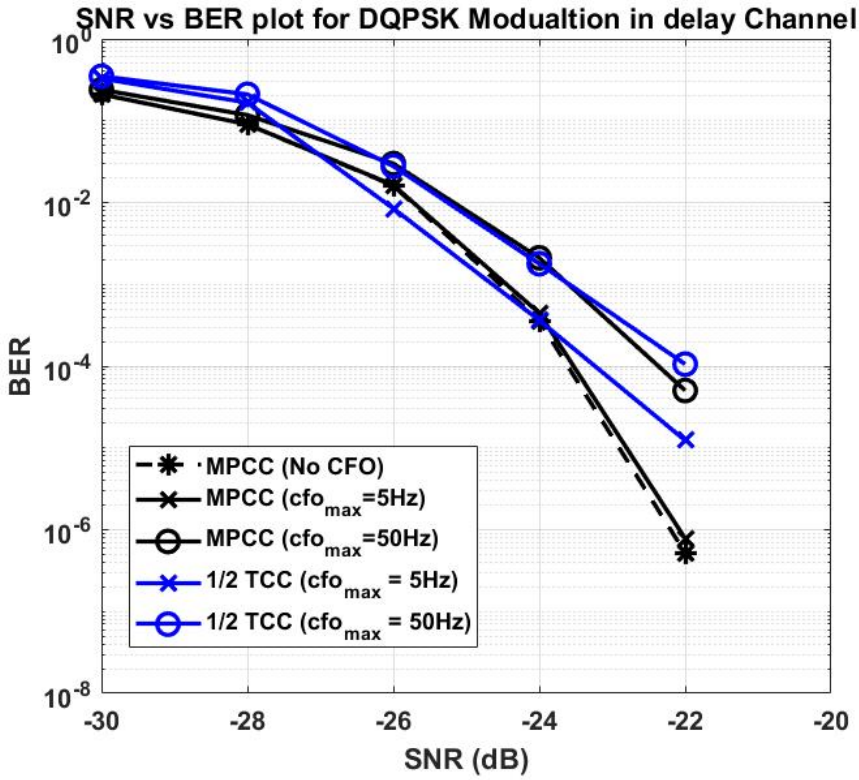

Figure 4.3: Average BER for Scenario 2 for rate 1/2

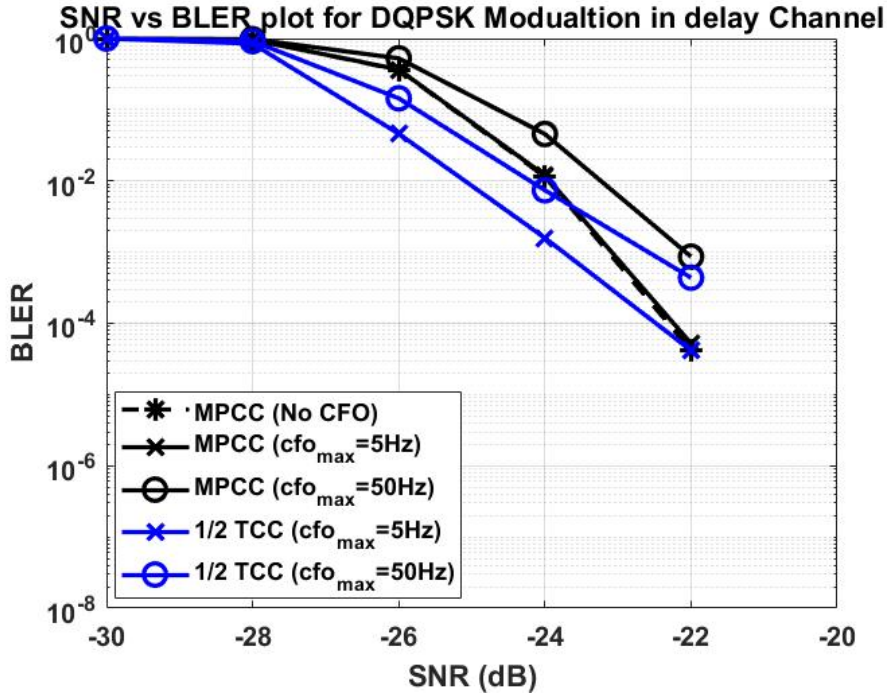

Figure 4.4: Average BLER for Scenario 2 for rate 1/2

For rate $\frac{2}{3}$:

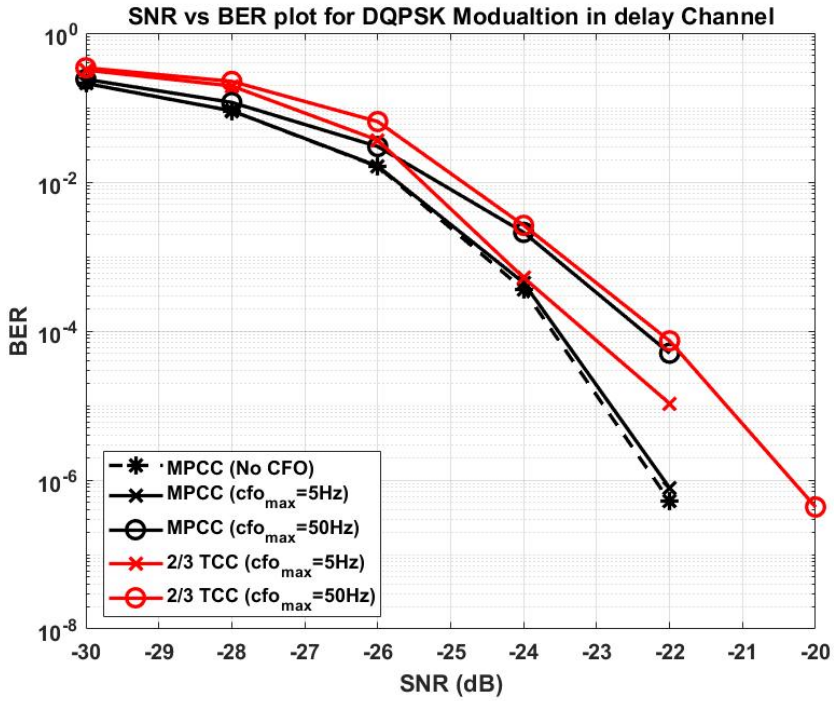

Figure 4.5: Average BER for Scenario 2 for rate 2/3

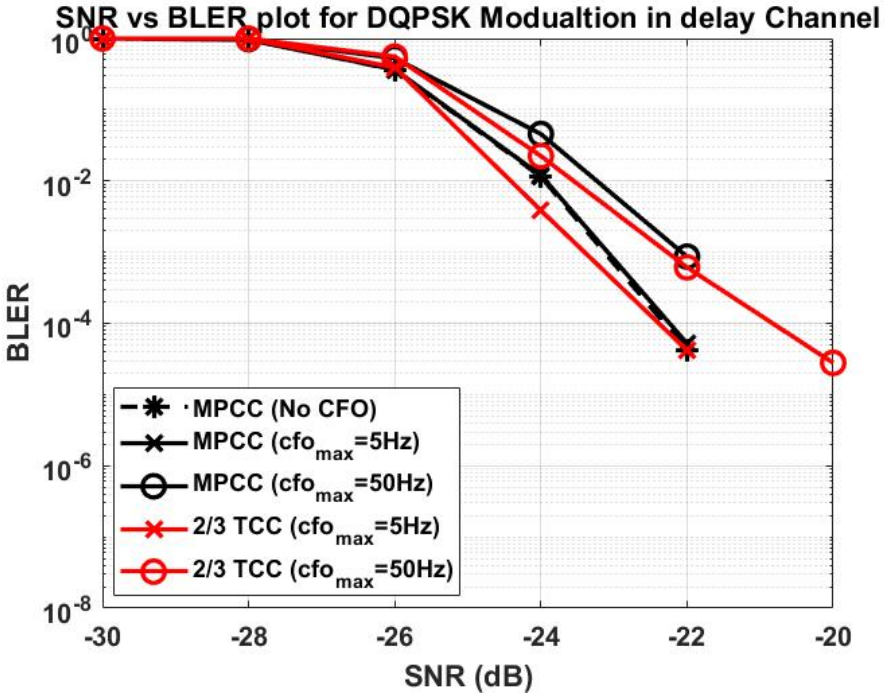

Figure 4.6: Average BLER for Scenario 2 for rate 2/3

4.4 SCENARIO 3

i. Power parameter, α_p for $(p \neq 1)$ modelled as continuous random variable sampled from $U\{-3dB, 0\}$
$\alpha_1 = 0$ such that the highest power user is always at 0 dB and system level SNR definition is still intact

ii. Residual CFO, $\Delta f_p = 0$ for all users

iii. Timing offset δ_p modelled as discrete random variable sampled from $U\{0, N_{CP}\}$

4.4.1 Results

Average BER and BLER are plotted.

For rate $\frac{1}{2}$:

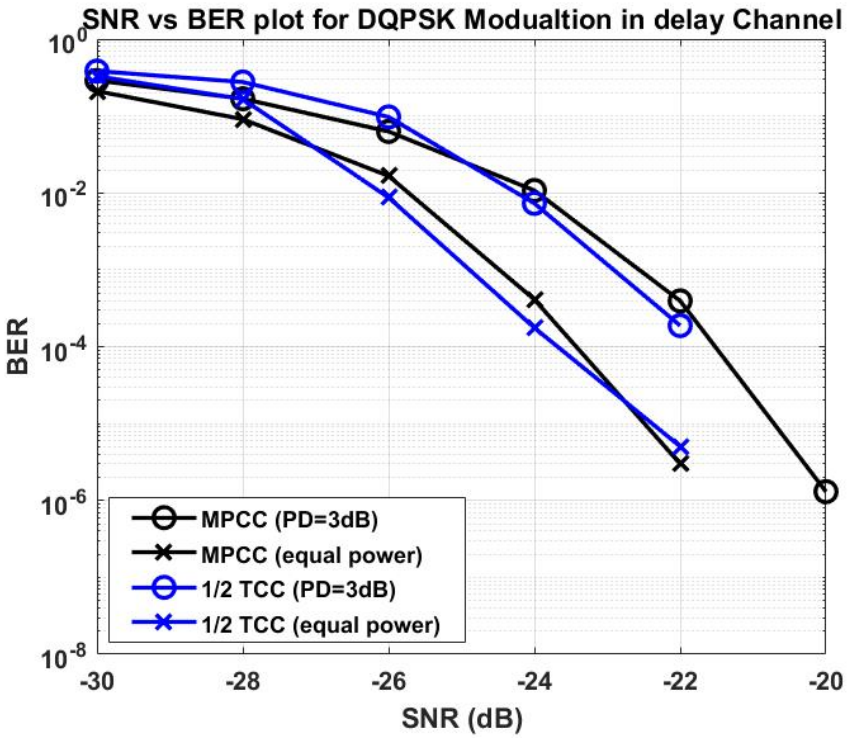

Figure 4.7: Average BER for Scenario 3 for rate 1/2

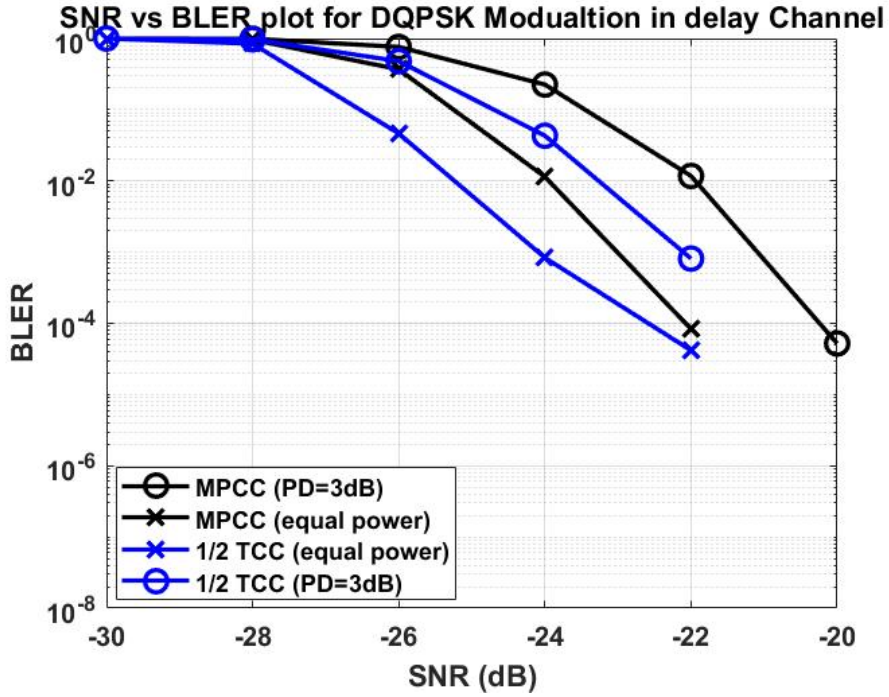

Figure 4.8: Average BLER for Scenario 3 for rate 1/2

For rate $\frac{2}{3}$:

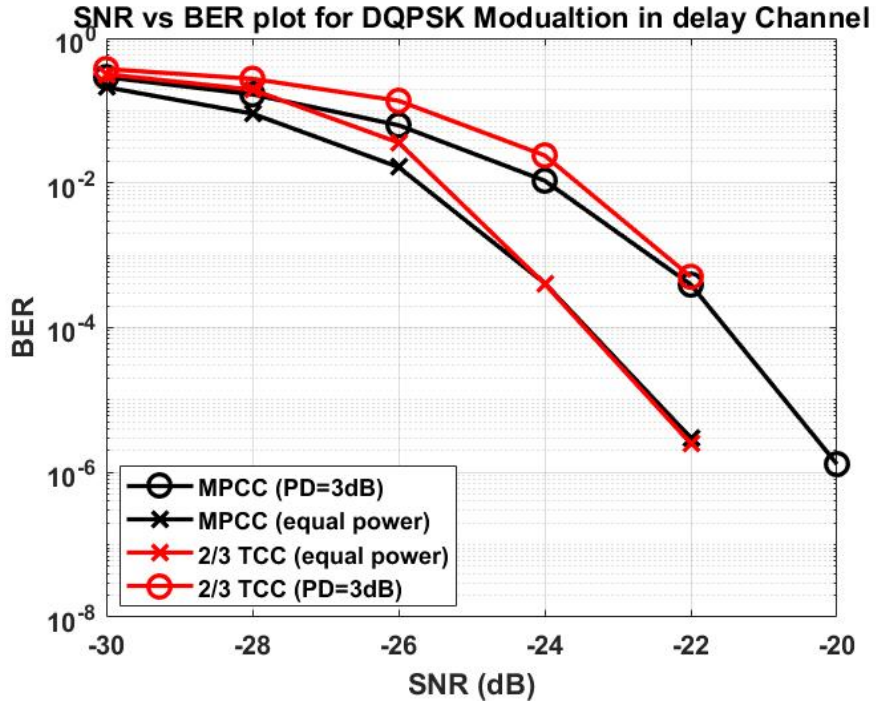

Figure 4.9: Average BER for Scenario 3 for rate 2/3

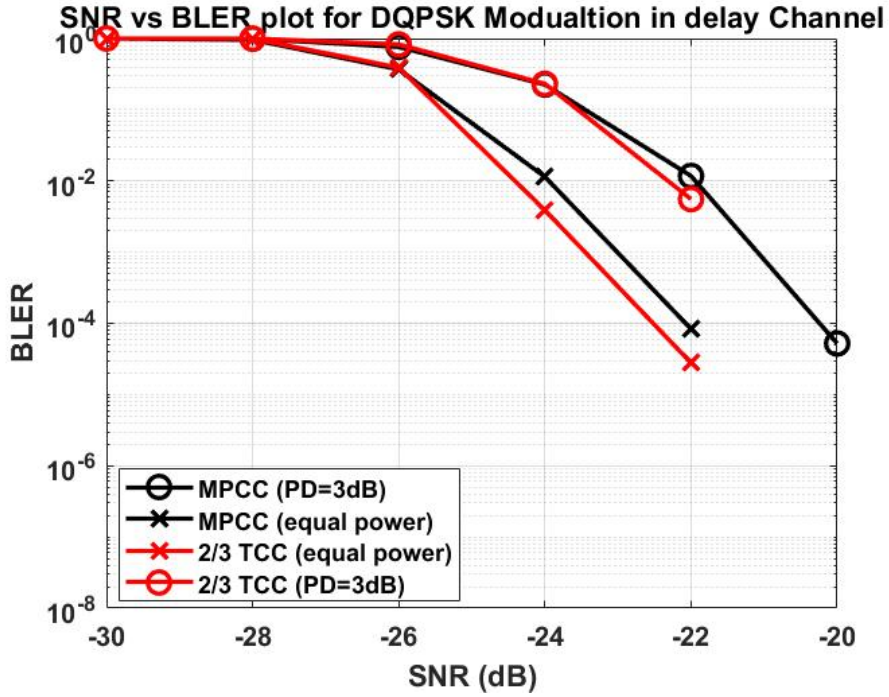

Figure 4.10: Average BLER for Scenario 3 for rate 2/3

4.5 SCENARIO 4

i. Power parameter, α_p for $(p \neq 1)$ modelled as continuous random variable sampled from $U\{-3dB, 0\}$

ii. Residual CFO, Δf_p modelled as discrete random variable sampled from $U\{-\Delta f_{max}, \Delta f_{max}\}$

iii. Timing offset δ_p modelled as discrete random variable sampled from $U\{0, N_{CP}\}$

4.5.1 Results

Average BER and BLER are plotted.

For rate $\frac{1}{2}$:

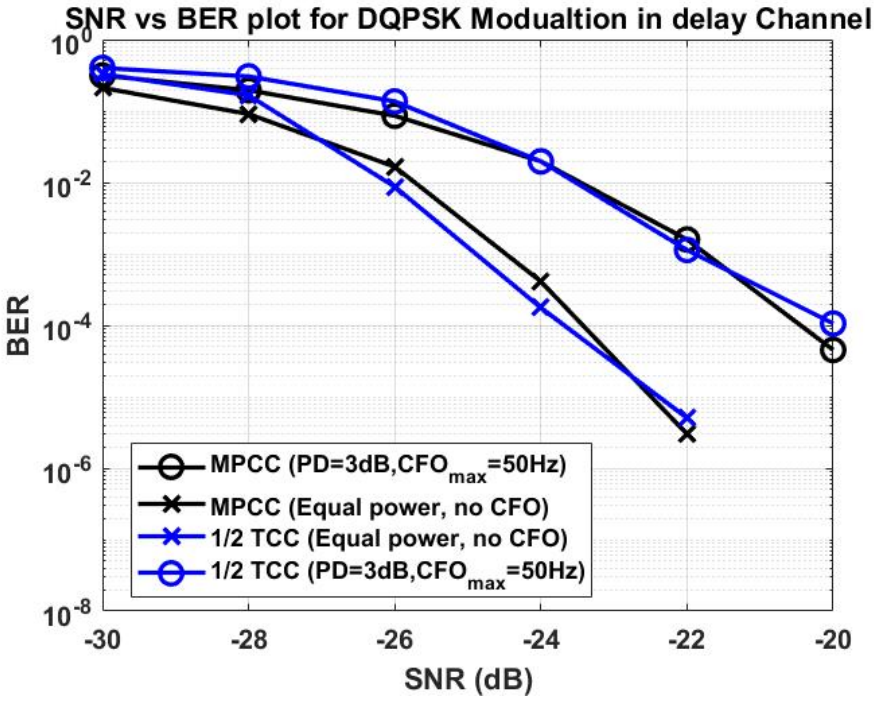

Figure 4.11: Average BER for Scenario 4 for rate 1/2

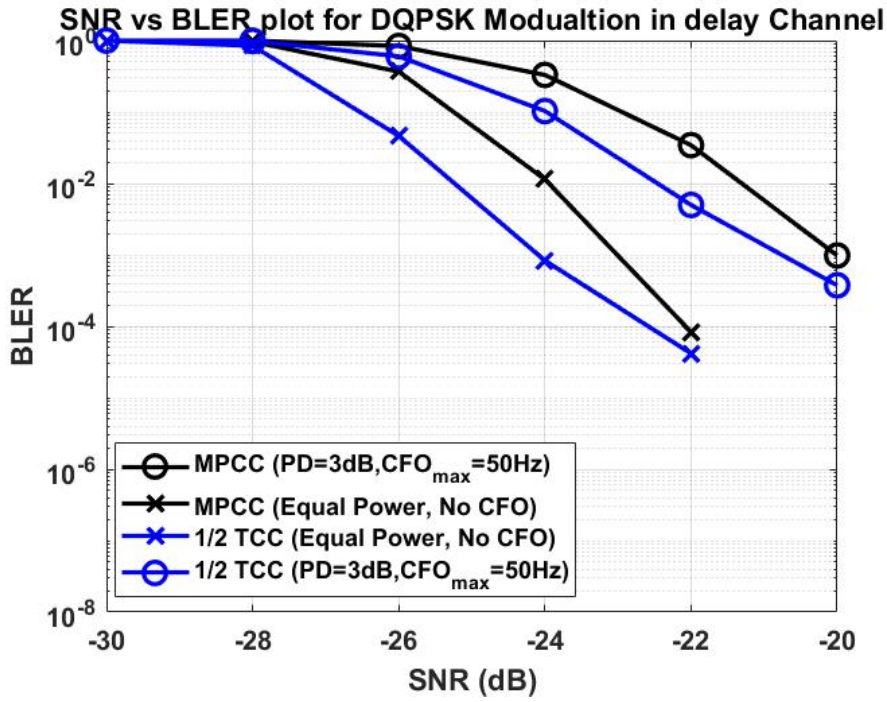

Figure 4.12: Average BLER for Scenario 4 for rate 1/2

For rate $\frac{2}{3}$:

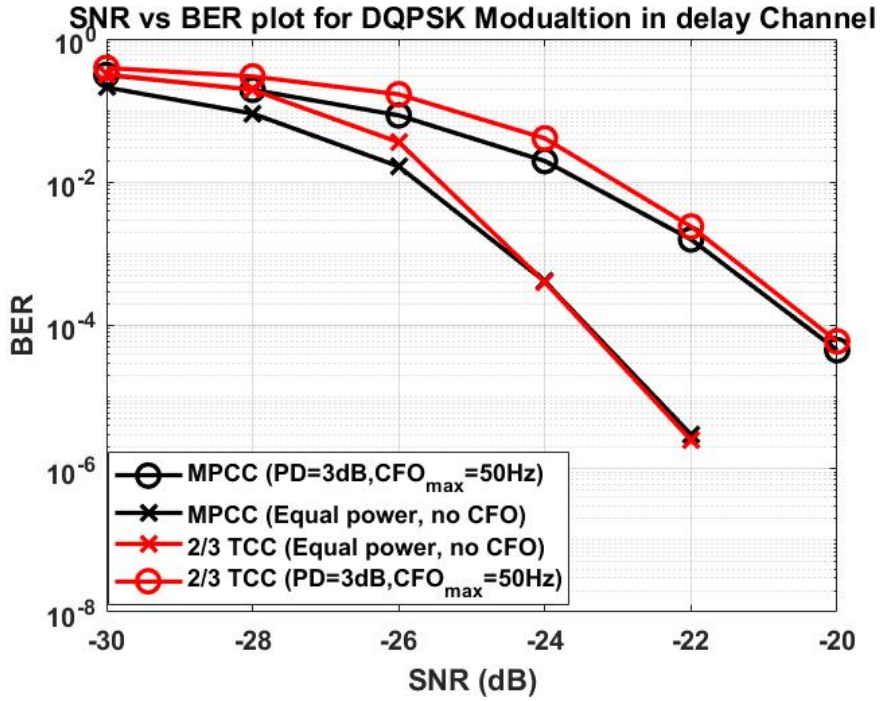

Figure 4.13: Average BER for Scenario 4 for rate 2/3

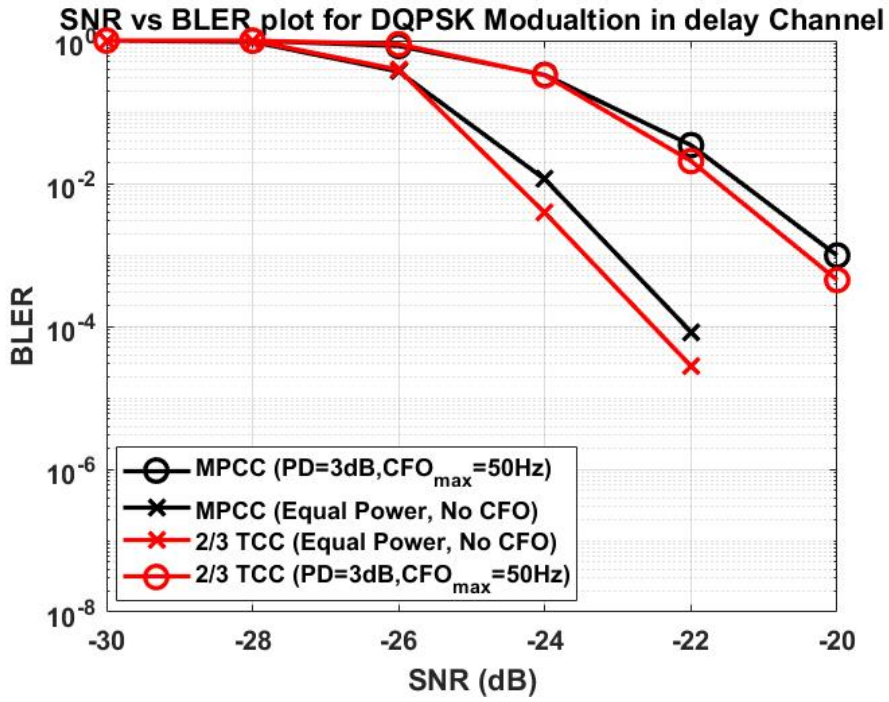

Figure 4.14: Average BLER for Scenario 4 for rate 2/3

CHAPTER 5

DQPSK AND LLRS

5.1 INTRODUCTION

Further extending the RCS approach of using DQPSK modulation system, we examined different methods of generating LLRs for the system and implemented them to check their simulation-level performance.

In a DQPSK symbol, the information bit is in the angle difference between two consecutive symbols. Consider,

$$r[k].r^*[k-1] = x[k].x^*[k-1] + x[k].n^*[k-1] + n[k].x^*[k-1] + n[k].n^*[k-1]$$

Based on the input used to calculate LLRs we have the following methods possible for DQPSK signal input.

5.1.1 Gaussian noise LLR

In this approach, the LLR is derived based on the probability density functions (pdf) of $r[k].r^*[k-1]$ conditioned on each possible value of the transmitted code bit. (4) We assume that all the other noise terms together in $r[k].r^*[k-1]$ have a Gaussian pdf.

$$r[k].r^*[k-1] \approx N(e^{j\theta}, \sigma_n^2)$$

where, θ is the angle difference between the $x[k]$ and $x[k-1]$.

This approach is an approximation but gives us but gives us similar performance compared to hard-decision decoding.

5.1.2 Partial Statistics LLR

In this, out of the four terms in

$$r[k].r^*[k-1] = x[k].x^*[k-1] + x[k].n^*[k-1] + n[k].x^*[k-1] + n[k].n^*[k-1]$$

, we ignore only the last term, $n[k].n^*[k-1]$.

Individually, those two terms,

$$x[k].n^*[k-1] \approx N(0, ||x[k]||^2\sigma_n^2)$$

$$x^*[k-1].n[k] \approx N(0, ||x^*[k-1]||^2\sigma_n^2)$$

The sum of these two random variables will also include their correlation term, which is mathematically proven to be equal to 0.

We know,

$$X \approx N(0, 2\sigma_x^2)$$
$$Y \approx N(0, 2\sigma_y^2)$$

We know,

$$\begin{aligned} Z &= X + Y \\ &\approx N(0, \sigma_x^2 + \sigma_x^2 + 2\rho\sigma_x\sigma_y) \end{aligned}$$

where,

$$\begin{aligned} \rho &= corr(X, Y) \\ &= \frac{cov(X, Y)}{\sigma_x\sigma_y} \end{aligned}$$

In our case, since $n[k]$ and $n^*[k-1]$ are uncorrelated, $\rho = 0$. Therefore,

$$x[k].n^*[k-1] + n[k].x^*[k-1] \approx N(0, 2\sigma_n^2)$$

and,

$$r[k].r^*[k-1] \approx N(e^{j\theta}, 2\sigma_n^2)$$

where, θ is the angle difference between the $x[k]$ and $x[k-1]$.

This gives us similar performance as the previous method but is statistically more accurate.

5.1.3 Joint pdf LLR

In this novel approach, (3) we use the joint conditional pdf,

$$p(r[k], r[k-1] \mid x[k], x[k-1])$$

The reason why we do this is that much information is lost in using the pdf, $\mathrm{p}(r[k].r^*[k-1])$ compared to using the joint pdf, $\mathrm{p}(r[k], r[k-1])$. Also, the product noise term in $\mathrm{p}(r[k].r^*[k-1])$ is assumed to have a Gaussian pdf, an approximation that further contributes to the inaccuracy of the metric. (4) On the other hand, the method proposed here is derived using the joint pdfs of the two consecutive received signals, conditioned on each possible value of the code bit concerned. This method outperformed the previous two methods.

$$
\begin{aligned}
& p(r[k], r[k-1] \mid x[k], x[k-1]) \\
& = p(r[k] \mid x[k]).p(r[k-1] \mid x[k-1]) \\
& \approx exp\{\frac{(r[k]-x[k]).(r^*[k]-x^*[k])}{-\sigma_n^2}\}.exp\{\frac{(r[k-1]-x[k-1]).(r^*[k-1]-x^*[k-1])}{-\sigma_n^2}\} \\
& = exp\{\frac{|r[k]|^2+|x[k]|^2-2R\{r[k].x^*[k]\}+|r[k-1]|^2+|x[k-1]|^2-2R\{r[k-1].x^*[k-1]\}}{-\sigma_n^2}\} \\
& = exp\{\frac{|r[k]|^2+1-2R\{r[k].x^*[k]\}+|r[k-1]|^2+1-2R\{r[k-1].x^*[k-1]\}}{-\sigma_n^2}\}
\end{aligned}
$$

This is directly used to calculate LLRs. Unlike the previous methods, LLR metrics are derived using the joint pdfs of the two consecutive received signals. This derivation does not require any assumptions on the pdfs and hence, performs better.

5.1.4 Max-log MAP with joint pdf LLR

The previous approach can be further simplified using Max-log MAP. This technique simplifies the MAP algorithm by transferring the recursions into the log domain and

invoking the approximation:

$$ln\left(\sum_i x_i\right) \approx max(x_i)\ \forall i$$

LLR, for joint PDF method includes,

$$\lambda_{i,j}[k] = ln\left(\sum exp\{\frac{|r[k]|^2 + 1 - 2R\{r[k].x^*[k]\} + |r[k-1]|^2 + 1 - 2R\{r[k-1].x^*[k-1]\}}{-\sigma_n^2}\}\right)$$

where, i denotes the bit position and j denotes the bit value. $i, j \in \{0, 1\}$

Let, $\{\phi_{i,j}\}$ represents the set of possible x[k] and x[k-1] which give that particular i and j. Therefore from the table below,

$$\phi_{0,0} \Leftrightarrow b_0 = 0$$

$$\phi_{0,1} \Leftrightarrow b_0 = 1$$

$$\phi_{1,0} \Leftrightarrow b_1 = 0$$

$$\phi_{1,1} \Leftrightarrow b_1 = 1$$

and only those 8 combinations of x[k] and x[k-1] corresponding to that particular bit are used to calculate bit-level LLR.

CASE	$e^{j.\Phi} = x[k].x^*[k-1]$	$x[k]$	$x[k-1]$
b_0[k]=0	$e^{j.0}$	$e^{j.\frac{\pi}{4}}$	$e^{j.\frac{\pi}{4}}$
		$e^{j.\frac{3\pi}{4}}$	$e^{j.\frac{3\pi}{4}}$
		$e^{-j.\frac{3\pi}{4}}$	$e^{-j.\frac{3\pi}{4}}$
		$e^{-j.\frac{\pi}{4}}$	$e^{-j.\frac{\pi}{4}}$
	$e^{j.\frac{\pi}{2}}$	$e^{j.\frac{\pi}{4}}$	$e^{-j.\frac{\pi}{4}}$
		$e^{j.\frac{3\pi}{4}}$	$e^{j.\frac{\pi}{4}}$
		$e^{-j.\frac{3\pi}{4}}$	$e^{j.\frac{3\pi}{4}}$
		$e^{-j.\frac{\pi}{4}}$	$e^{-j.\frac{3\pi}{4}}$
b_0[k]=1	$e^{j.\pi}$	$e^{j.\frac{\pi}{4}}$	$e^{-j.\frac{3\pi}{4}}$
		$e^{j.\frac{3\pi}{4}}$	$e^{-j.\frac{\pi}{4}}$
		$e^{-j.\frac{3\pi}{4}}$	$e^{j.\frac{\pi}{4}}$
		$e^{-j.\frac{\pi}{4}}$	$e^{j.\frac{3\pi}{4}}$
	$e^{-j.\frac{\pi}{2}}$	$e^{j.\frac{\pi}{4}}$	$e^{j.\frac{3\pi}{4}}$
		$e^{j.\frac{3\pi}{4}}$	$e^{-j.\frac{3\pi}{4}}$
		$e^{-j.\frac{3\pi}{4}}$	$e^{-j.\frac{\pi}{4}}$
		$e^{-j.\frac{\pi}{4}}$	$e^{j.\frac{\pi}{4}}$
b_1[k]=0	$e^{j.0}$	$e^{j.\frac{\pi}{4}}$	$e^{j.\frac{\pi}{4}}$
		$e^{j.\frac{3\pi}{4}}$	$e^{j.\frac{3\pi}{4}}$
		$e^{-j.\frac{3\pi}{4}}$	$e^{-j.\frac{3\pi}{4}}$
		$e^{-j.\frac{\pi}{4}}$	$e^{-j.\frac{\pi}{4}}$
	$e^{-j.\frac{\pi}{2}}$	$e^{j.\frac{\pi}{4}}$	$e^{j.\frac{3\pi}{4}}$
		$e^{j.\frac{3\pi}{4}}$	$e^{-j.\frac{3\pi}{4}}$
		$e^{-j.\frac{3\pi}{4}}$	$e^{-j.\frac{\pi}{4}}$
		$e^{-j.\frac{\pi}{4}}$	$e^{j.\frac{\pi}{4}}$
b_1[k]=1	$e^{j.\frac{\pi}{2}}$	$e^{j.\frac{\pi}{4}}$	$e^{-j.\frac{\pi}{4}}$
		$e^{j.\frac{3\pi}{4}}$	$e^{j.\frac{\pi}{4}}$
		$e^{-j.\frac{3\pi}{4}}$	$e^{j.\frac{3\pi}{4}}$
		$e^{-j.\frac{\pi}{4}}$	$e^{-j.\frac{3\pi}{4}}$
	$e^{j.\pi}$	$e^{j.\frac{\pi}{4}}$	$e^{-j.\frac{3\pi}{4}}$
		$e^{j.\frac{3\pi}{4}}$	$e^{-j.\frac{\pi}{4}}$
		$e^{-j.\frac{3\pi}{4}}$	$e^{j.\frac{\pi}{4}}$
		$e^{-j.\frac{\pi}{4}}$	$e^{j.\frac{3\pi}{4}}$

Figure 5.1: All possible consecutive symbols for a particular bit and position value

Using Max-log MAP approximation for a given $\phi_{i,j}$,

$$\lambda_{i,j}[k] = ln\left(\sum exp\{\frac{|r[k]|^2 + 2 - 2R\{r[k].x^*[k]\} + |r[k-1]|^2 - 2R\{r[k-1].x^*[k-1]\}}{-\sigma_n^2}\}\right)$$
$$\approx max\left(exp\{\frac{|r[k]|^2 + 2 - 2R\{r[k].x^*[k]\} + |r[k-1]|^2 - 2R\{r[k-1].x^*[k-1]\}}{-\sigma_n^2}\}\right)$$
$$\approx max\left(\frac{|r[k]|^2 + 2 - 2R\{r[k].x^*[k]\} + |r[k-1]|^2 - 2R\{r[k-1].x^*[k-1]\}}{-\sigma_n^2}\right)$$

Now, $\phi_{i,j}$ is independent of $|r[k]|$ and $|r[k-1]|$, and the $\lambda_{i,j}$ reduces to,

$$\lambda_{i,j}[k] \approx max\left(\frac{-2R\{r[k].x^*[k]\} - 2R\{r[k-1].x^*[k-1]\}}{-\sigma_n^2}\right)$$
$$\approx max\left(\frac{2R\{r[k].x^*[k]\} + 2R\{r[k-1].x^*[k-1]\}}{\sigma_n^2}\right)$$

here,

$$R\{r[k].x^*[k]\} = r_R[k].x_R[k] + r_{Im}[k].x_{Im}[k]$$

and

$$R\{r[k-1].x^*[k-1]\} = r_R[k-1].x_R[k-1] + r_{Im}[k-1].x_{Im}[k-1]$$

Therefore,

$$\lambda_{i,j}[k] \approx max\,(2(r_R[k].x_R[k] + r_{Im}[k].x_{Im}[k] + r_R[k-1].x_R[k-1] + r_{Im}[k-1].x_{Im}[k-1]))$$

Therefore, for each i and j, we can determine from the above table, which particular x[k] and x[k-1] are to be considered.

5.2 SIMULATION RESULTS

Both the coded and uncoded BER results were plotted.

5.2.1 Observations

i. Both the Gaussian noise assumption method and Partial statistics method perform the same for both coded and uncoded results.

ii. In the uncoded BER plot, Gaussian noise assumption method and Partial statistics

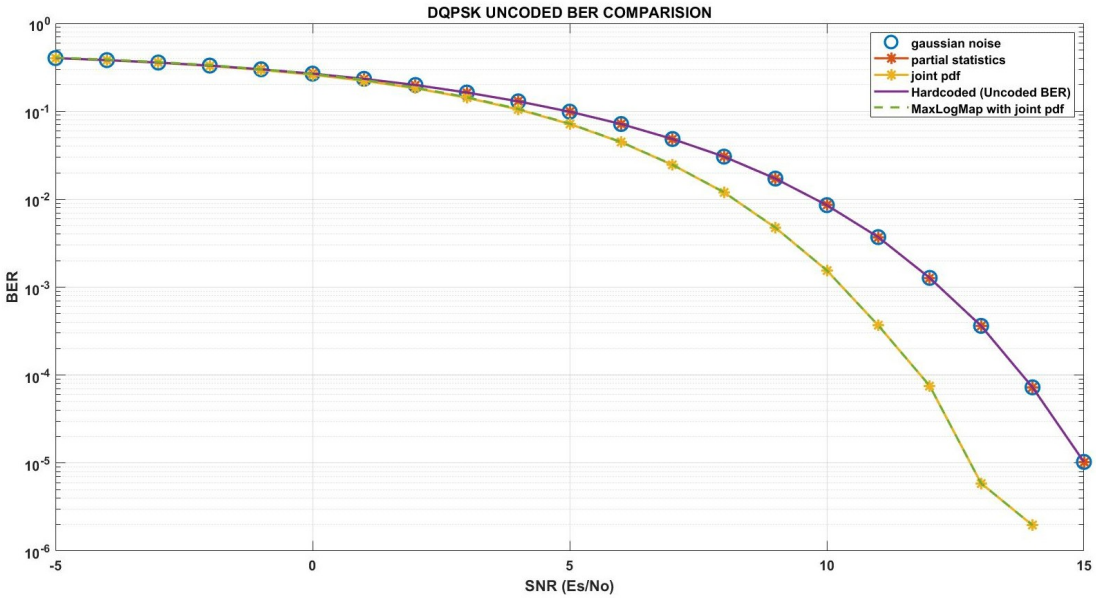

Figure 5.2: Uncoded BER for different LLR methods

method perform similar to the hardcoded method (which doesn't use LLRs).

iii. As expected, Joint-pdf method performs the best for both coded and uncoded results.

iv. Max-log MAP method for joint-pdf reduced the number of computations needed to calculate the rate at no cost in performance and has the same result as the joint-pdf method.

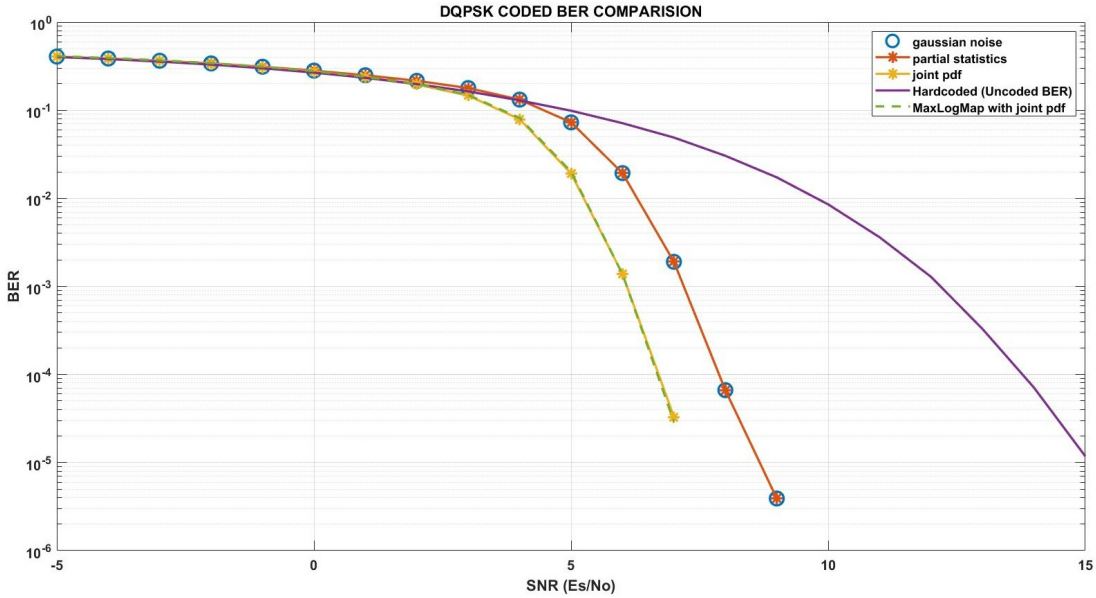

Figure 5.3: Coded BER for different LLR methods

CHAPTER 6

CONCLUSION

The thesis set out to understand the various satellite communication systems. The two-phase three-way relay system study and the RCS project helped me get a tighter hold on the subject. In the 2-way 3-phase relay system study, we introduced the concept of constellation shaping to better decode the user's data even in the presence of interference. A joint-LLR generation technique was used to decode user data even in the presence of an interferer efficiently. An OFDM system model was designed for the comparison study keeping the system throughput the same in all the scenarios. The simulation results proudly proved the spectral efficiency in the interference scenario versus the no interference scenario. The comparison between the no ideal self-cancellation scenario and self-cancellation case with hub repetition showed the same BER performance and spectral efficiency. The two-phase three-way relay system can also be extended to two-phase N-way relay by using an N-square QAM as a reference constellation for effective decoding.

The role of Turbo codes in improving BER performance under various signal impairments was also computed. This FEC scheme has been successfully integrated into the reverse link of the RCS project. To better understand the bit-level LLR generation in a DQPSK modulated system, a few novel techniques to calculate LLRs for DQPSK modulated signal were proposed. A comparison between these methods (Gaussian noise methods, partial statistics method, joint-pdf method, and Max-log MAP on joint-pdf method) showed that the joint-pdf method outperformed others in coded and uncoded BER plots. Max-log MAP on the joint-pdf method was computationally less extensive but showed the same result as the joint-pdf method.

There is a scope for numerous applications for the same. Apart from this, a full lab-scale hardware demo of the RCS project using Zynq Ultrascale MPSoc and ADRV 9009 is also in progress and it includes the latest FEC integration in both forward and reverse link.

APPENDIX A

TURBO CODES

A.1 INTRODUCTION

One of the most used channel codes are convolutional codes, with the decoding strategy based on the Viterbi algorithm. The advantages of convolutional codes are used in Turbo Codes (TC), which can achieve performances within a 2 dB of channel capacity. These codes are parallel concatenation of two Recursive Systematic Convolutional (RSC) codes separated by an interleaver. The performances of the turbo codes are due to parallel concatenation of component codes, the interleaver schemes and the iterative decoding using the Soft Input Soft Output (SISO) algorithms. (2)

A.2 TURBO ENCODER

The Turbo encoder is composed of two Recursive Systematic Convolutional (RSC) encodes, which are usually identical. The first encoder operates on the input bits represented by the frame **u**, in their original order while the second one operates on the input bits which are permuted by the interleaver frame **u'**. The output of the turbo-encoder frame is represented by:

$$\mathbf{v} = (\mathbf{u}, c_1, c_2)$$

where frame c_1 is the output of the first RSC and frame c_2 is the output of the second RSC. If the input frame **u** is of length k and the output frame **v** is of length n, then the encoder rate is $R = k/n$. (1)

For block encoding data is segmented into non-overlapping blocks of length k with each block encoded (and decoded) independently. This scheme imposes the use of a block interleaver with the constraint that the RSC's must begin in the same state for each new

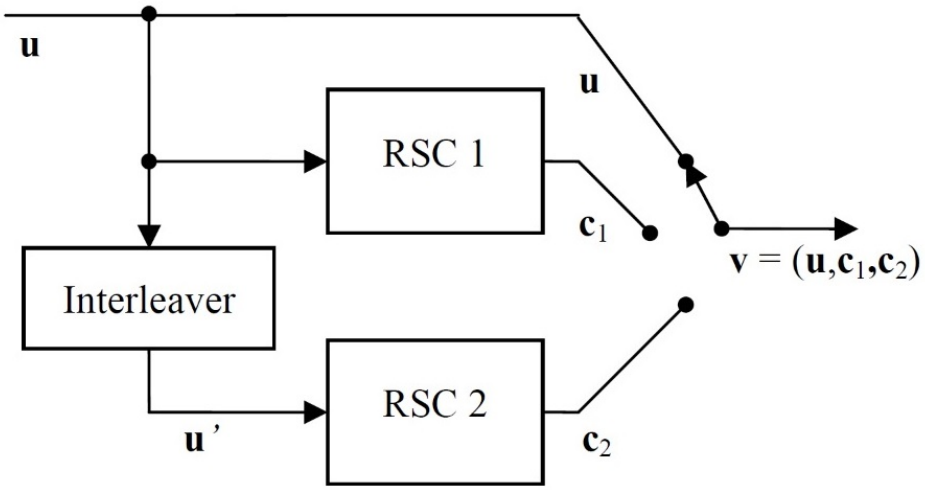

Figure A.1: Turbo encoder for rate $\frac{1}{3}$

block. This requires either trellis termination or trellis truncation. Trellis termination need appending extra symbols (usually named tail bits) to the input frame to ensure that the shift registers of the constituent RSC encoders starts and ends at the same zero state. If the encoder has code rate 1/3, then it maps k data bits into 3k coded bits plus 3m tail bits. Trellis truncation simply involves resetting the state of the RSC's for each new block.

The interleaver used for parallel concatenation is a device that permutes coordinates either on a block basis (a generalized "block" interleaver) or on a sliding window basis (a generalized "convolutional" interleaver). The interleaver ensures that the set of code sequences generated by the turbo code has nice weight properties, which reduces the probability that the decoder will mistake one codeword for another.

Notably, turbo codes perform well at low SNR because the number of low-weight code words is small. This is ideal for the code because high weight code words result in better decoder performance. The performance of turbo codes at high SNR is limited by the relatively small distance of the code.

A.3 LOG-LIKELIHOOD RATIOS

After the encoded data is modulated and passed through the channel, it is used to generate LLRs. These LLRs serve as an input to the Turbo decoder. Bit level Log-likelihood ratio is defined as:

$$L(b) = log\frac{\Pr(b=0|r)}{\Pr(b=1|r)}$$

For equal probability of all symbols under AWGN channel scenario, this modifies to:

$$L(b) = log\frac{\sum_{s\in S_0} e^{-\frac{(x-s_x)^2+(y-s_y)^2}{\sigma^2}}}{\sum_{s\in S_1} e^{-\frac{(x-s_x)^2+(y-s_y)^2}{\sigma^2}}}$$

where,

b is the bit for which the LLR is being calculated,

(x,y) are the coordinates of the received signal r,

(s_x, s_y) are the coordinates of the ideal symbol,

σ^2 is the noise variance of the signal,

S_0 and S_1 represents the ideal symbols with bit 0 and bit 1 at the given bit position, respectively.

A.4 TURBO DECODER

These bit-level LLRs are passed through the turbo decoder.

Let be the received sequence of length n , $\mathbf{y} = (y^s, y^{p1}, y^{p2})$, where the vector $\mathbf{y^s} = (y_1^s, y_2^s, \cdots, y_n^s)$ is formed only by the received information symbols, and the vectors $\mathbf{y^{p1}} = (y_1^{p1}, y_2^{p1}, \cdots, y_n^{p1})$ and $\mathbf{y^{p2}} = (y_1^{p2}, y_2^{p2}, \cdots, y_n^{p2})$ represents the received parity symbols.These three streams are passed to the input of the turbo decoder as shown. (2) At any time, the decoder1 uses the partial received information to make its decisions and outputs the *a posteriori information* which is used to compute the *extrinsic information*. Decoder2 uses this *extrinsic information* along with the received information to make its decision. Decoder1 uses this output from decoder2 as a part of its input. Therefore,

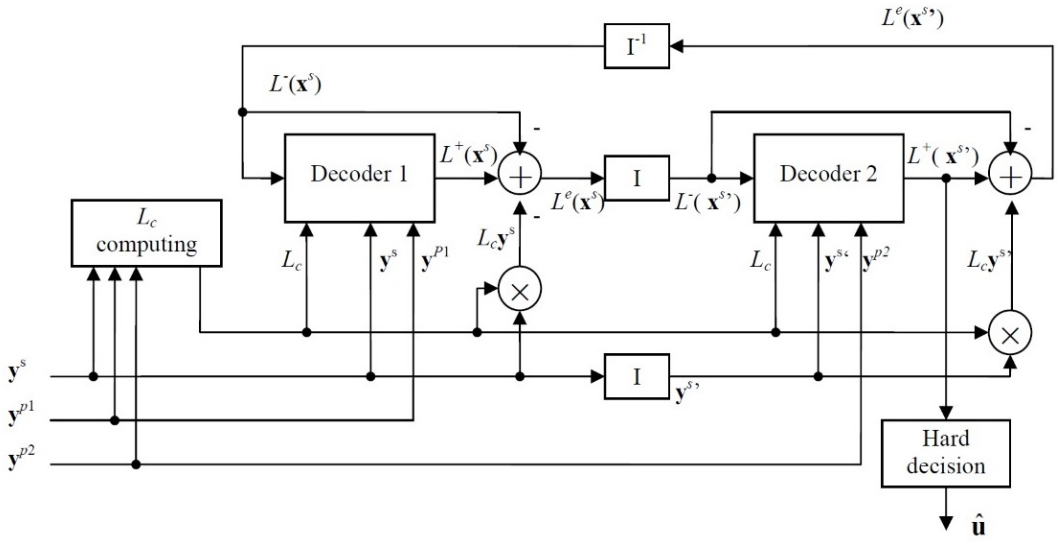

Figure A.2: Turbo decoder

in the second iteration, the first decoder decodes the same channel symbols, but now with additional information about the value of the input symbols provided by the second decoder in the first iteration. After some iterations, the algorithm converges and the extrinsic information values remains the same. Now the decision about the message bits $\hat{\mathbf{u}}$ is made based on the *a posteriori values* from decoder 2.

REFERENCES

[1] H. Jin, R. J. McEliece, “Coding Theorems for Turbo Code Ensembles”, IEEE Trans. Inform. Theory, vol. 48, No. 6, pp. 1451-1463, June 2002.

[2] Perisoara, Lucian & Stoian, Rodica. (2008). The Decision Reliability of MAP, Log-MAP, Max-Log-MAP and SOVA Algorithms for Turbo Codes. 2. 65-74.

[3] E. Mo and P. Y. Kam, "Log-Likelihood Metrics Based on Two-Symbol-Interval Observations for LDPC Codes with BDPSK Transmission," 2008 IEEE 68th Vehicular Technology Conference, 2008, pp. 1-5, doi: 10.1109/VETECF.2008.159.

[4] E. Mo, P. Y. Kam and M. A. Armand, "LLR metrics for LDPC codes with quadrature differential PSK transmission, and their performances," 2008 International Symposium on Information Theory and Its Applications, 2008, pp. 1-6, doi: 10.1109/ISITA.2008.4895388.